Aircraft induced cirrus cloud

First year report

Trinity 2006

Atmospheric, Oceanic & Planetary Physics

Clarendon Laboratory

University of Oxford

M Raveem Tahir

St Edmund Hall

Printed 19th September 2006
Typeface Computer Modern 12 pt
System LaTeX 2_ε

Abstract

An approach has been formulated whereby two models are used to produce global maps of aircraft induced cirrus. A contrail model with an intake of atmospheric conditions and flight paths, applies the Schmidt-Appleman criterion in every cell to ascertain whether the conditions are suitable for contrail formation. If they are, then a microphysical model operates, simulating the life cycle of aerosol and ice particles: nucleation, condensation and coagulation. A resulting size distribution of ice crystals is deemed indicative of contrail cirrus cloud formation. The aim is to then use a third model to compare such a map of contrail cirrus to established and new climatologies of cirrus clouds, thus quantifying the anthropogenic contribution to cirrus trends.

Contents

List of Figures

List of Tables

Glossary

CA Cloud Amount

CCN Cloud Condensation Nuclei

ECMWF European Centre for Medium range Weather Forecasts

EI Emission Index

ERA40 **E**CMWF **40** year **r**e-**a**nalysis

GOES Geostationary Operational Environmental Satellite

GRAPE Global Retrieval of ATSR cloud Parameters and Evaluation

HIRS High resolution Infrared Radiation Sounder

IPCC Intergovermental Panel on Climate Change

ISCCP International Satellite Cloud Climatology Project

MIPAS Michelson Interferometer for Passive Atmospheric Sounding

NCEP National Centers for Environmental Prediction

NMHCs **N**on-**m**ethane **h**ydro**c**arbons

NOAA National Oceanic and Atmospheric Administration

SAMM Stratospheric Aerosol Microphysical Model

TRADEOFF Aircraft emissions: contribution of different climate components to changes in radiative forcing - **tradeoff** to reduce atmospheric impact

TIROS Television and IR Observations Satellite

TOVS TIROS Operational Vertical Sounder

UTLS Upper Troposphere / Lower Stratosphere

UTH Upper Troposphere Humidity

WMO World Meteorological Organisation

Chapter 1

Introduction

Contrail cirrus from aviation increases the total amount of global cirrus, but to what extent remains uncertain. Cirrus cloud influence the climate system, however, estimates of the global radiative forcing attributable to cirrus are very poor [Penner et al., 1999]. Any anthropogenic increase in cirrus cloud cover therefore needs to be quantified. This will allow discussion of aviation's contribution to global warming and of mitigation techniques, should they become necessary.

Contrails from aircraft may eventually form cirrus which is considered indistinguishible[1] from cirrus which forms naturally. The magnitude of contrail cirrus cover lies between two limits [Minnis, 2005, Minnis et al., 2003]:

- The *lower limit* is remote sensing of linear cirrus which has formed from contrails and remained undisturbed, retaining its geometric signature. This assumes that such data do not suffer from false positives: it has occasionally been known for natural cirrus to form linearly [Gierens, 2006b].
- The *upper limit* assumes that all cirrus trends (mean changes in cirrus coverage over time) are due to aircraft. This is by nature problematic since it assumes that the "natural" cirrus amount remains constant or is known. A decrease in global cirrus coverage would also make this upper limit nonsensical.

Without a method for discriminating to which degree the cirrus trend exceeding line-shaped cirrus is aircraft induced, we cannot draw conclusions about the climatic impact arising from contrail cirrus. Remote sensing cannot serve to quantitatively assign a value between these two limits, therefore we must model, using the best possible data, the emissions to contrails to cirrus transition.

This project aims to produce global maps of aircraft induced cirrus with a focus on microphysical modelling of contrail evolution. It is motivated by the prospect of quantifying the anthropogenic cirrus contribution towards global cirrus coverage trends. Since the method will be based on ambient physical parameters, flight inventories and

[1] *In situ* measurements can sometimes show that contrail cirrus contains soot concentrations noticably in excess of "natural" cirrus [Gierens, 2006b]. However, since cirrus trends require global rather than local information, remote sensing of cirrus must be used instead. It is then impossible to make the fine distinction between contrail and natural cirrus that *in situ* data afford.

established algorithms designed for simulating steps in the contrails to cirrus evolution, such a tool will prove useful in lifting the uncertainty that yet surrounds the short and long term effects produced by contrail cirrus.

The targets for the first year are to establish a schedule for expected progress over the next two years and become familiar with methods, literature, models and problems associated with contrail to cirrus modelling. Specific goals therefore comprise:

- To formulate a plan whereby the aim is divided into component tasks, each of which is clearly defined according to the data set, published algorithm or general method required to accomplish that task.
- To start updating the existing model, SAMM, so that it becomes capable of simulating the microphysical processes occurring in aircraft plumes.
- To create a model which can predict contrail occurrence.
- To start investigating cirrus climatologies for eventual comparison with model output.

Chapter 2

Cirrus

Cirrus are high thin and wispy ice clouds which cover about 35% of the Earth's surface [Tabazadeh et al., 1997]. Their appearance from the Earth's surface is exemplified in Figure 2.0.1.

Figure 2.0.1: Characteristic cirrus [Met Office, 2006, NASA, 2006, *Unknown*, 2006].

2.1 Formation

Cirrus inhabit the upper troposphere (>∼8 km) where it is so cold (generally below -30°C) that cloud droplets are only transient and cannot be primarily reponsible for cirrus generation [Heymsfield and McFarquhar, 2002]. Whilst still poorly understood, it is now accepted that the precursors of cloud droplets (haze particles composed of aqueous solutions) are involved in cirrus production. It has been suggested that a distinguishible feature of cirrus is the background aerosol (aqueous H_2SO_4 droplets) in a relatively clean upper troposphere, on which cirrus ice crystals can nucleate [Sassen, 2002, Tabazadeh et al., 1997]. Another source for ice formation is when supercooled droplets encounter "foreign" nuclei lifted from the boundary layer, initiating freezing.

Cirrus formation therefore occurs mainly due to updrafts (from the cm s^{-1} to the m s^{-1} scale) which lift moist air and haze particles. Adiabatic expansion leads to cooling and ice particle formation occurs with the aid of haze nuclei. Cirrus can also form from the top down where gravitational settling propagates ice particles downwards. Figure 2.1.1 shows how cirrus forms a *head cell* from updrafts, which leads to characteristically long streamers of precipitation-sized ice particles, from which further updrafts can create new cirrus turrets [Starr and Quante, 2002].

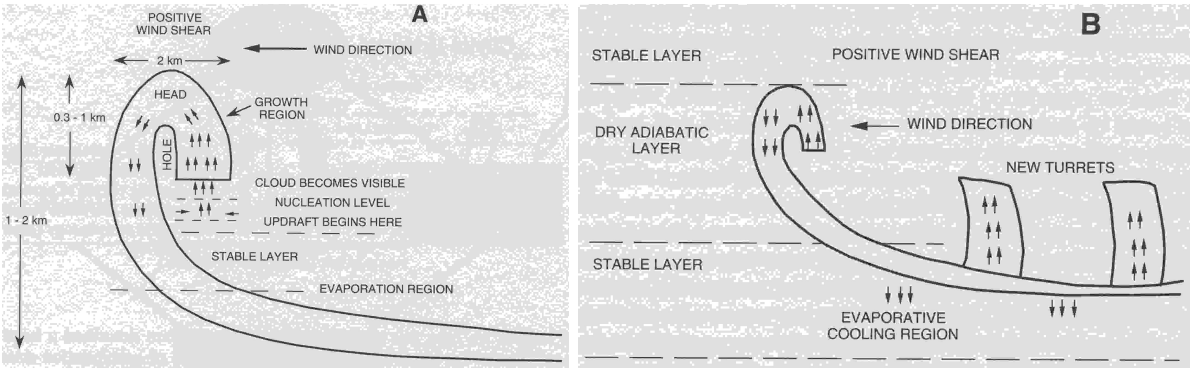

Figure 2.1.1: Schematic diagrams from Heymsfield [1975], showing characteristic shape, dimensions and processes of cirrus in wind shear.

2.2 Radiative effects

Early work by London, Moller, Kondratyev and Manabe in the fifties and sixties demonstrated the important radiative effect of cirrus clouds on the global heat budget and therefore in the climate system. Cirrus give rise to two opposing radiative processes: they can act as a thermal blanket by restricting outgoing infrared radiation and they can also be effective at reflecting incoming solar radiation back into space. The nature of the balance between the albedo and greenhouse effect determines the net impact of cirrus upon the climate system. Which process dominates appears to be quite sensitive to cloud microphysical and macrophysical properties, which may in turn be dependent on local weather processes and geographic location. Cirrus play a significant role in regulating the balance of the earth-atmosphere system and are therefore a crucial component in understanding anthropogenic climate change: a current concern being whether jet aircraft traffic is creating more cirrus cloud cover.

2.3 The problems of definition and measurement

Cloud classification took a large step forwards when Hildebrandsson and Abercrombie produced the first comprehensive classification in 1887 of five families and ten genera, based on height. Their work, which introduced *low*, *middle* and *high* as useful classification overlays, became the standard in cloud physics and continues to remain relavent to the present day. The criteria for cirrus identification have therefore traditionally relied upon visual appearance, including structure and colour, which make them distinct from clouds in the lower and middle troposphere.

The definition of cirrus[1] has not changed very much in over a century and the search continues for a definition which is physical rather than being based on morphology and colour. Many measurements, *in situ* and remote have been taken of cirrus over the decades, resulting in data on radiative, chemical and physical attributes, but a unique set of properties by which cirrus can be exclusively defined has remained elusive.

[1]Literally *curl of hair*. The term originated from L Howard's 1803 cloud classification [Lynch, 2002].

The *two-parameter classification* was a concept created after satellite measurements (from the Geostationary Operational Environmental Satellite (GOES) and the Television and IR Observations Satellite (TIROS) platforms) allowed clouds to be labelled as *bright* or *dark* in the visible and *hot* or *cold* in the infrared (Figure 2.3.1).

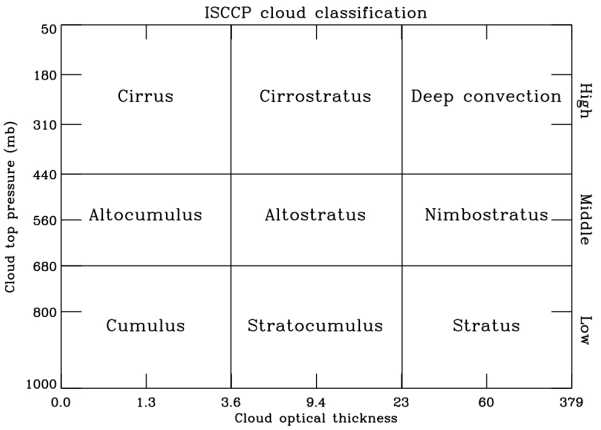

Figure 2.3.1: ISCCP radiometric cloud classification after Rossow et al. [1996].

Cirrus was classed as dark (or thin) and cold due to low optical thickness and low temperature. This classification is not, however, a definition, but a convenient way of sorting clouds purely by their radiative attributes, which correlate in some degree to the visual descriptions. It is therefore not a perfect means by which to identify cirrus. Despite this, the definitions in Figure 2.3.1 have been used by the International Satellite Cloud Climatology Project (ISCCP) to produce global climatologies for all cloud types, including cirrus. To date, three properties (albeit without limits) have been qualitatively associated by the meteorological community with cirrus [Lynch, 2002]:

- A large ice content. Cirrus are composed predominantly or wholly of ice wereas the majority of other clouds consist of water droplets. Most genera of cloud can contain ice: *all cirrus clouds are ice, but not all ice clouds are cirrus.*

- A high altitude. Cirrus comprise the highest tropospheric cloud category

- A small optical depth. The World Meteorological Organisation (WMO) defines cirrus as "*Detached clouds in the form of white, delicate filaments or white or mostly white patches or narrow bands. These clouds have a fibrous (hair-like) appearance, or a silky sheen, of both.*"

Cirrostratus and *cirrocumulus* have also been (visually) defined by the WMO. Two types without formal WMO classification are *subvisual*[2] and *contrail* cirrus, both well recognised meteorologically, contrail cirrus being a focus of this current work.

Quantitative measurements of cirrus cloud radiative and microphysical properties started being acquired and analysed in the late sixties and seventies by meteorologists. The main drawback of existing *in situ* instrumentation is the inability to effectively characterise small particles (< 200 nm). Cirrus detection also remains a challenge for satellite cloud retrieval: since the traditional definition of cirrus has been on visual appearance from the ground (a practise in use for over a century), appreciable new problems are created when cloud systems are viewed from above by cameras. These include accounting for cloud fraction, spatial inhomogeneity, correctly characterising background radiances for clear sky, surface and lower cloud, understanding non-spherical

[2]Subvisual cirrus is defined as cirrus with an optical depth of less than 0.03 in the visible and may be nearly ubiquitous [Lynch, 2002].

ice particle scattering behaviour, inferring cloud optical depth and maintaining accurate instrument calibration. More fundamental are the cirrus clouds which escape detection because they are too thin and the tops of deep cloud systems which are sometimes wrongly classified as cirrus.

Many of the problems associated with identifying and measuring cirrus are wholly duplicated in attempts to detect contrail cirrus once it loses its linear structure.

Chapter 3

Contrails

Condensation trails or contrails[1] are the linear white cloud-like formations often observed in the wake of a passing aeroplane. They form in two ways:

i. Aerodynamic contrails can result from vortices produced by certain parts of the plane. For a brief description, see Appendix C.

ii. Thermodynamic contrails are those which are triggered by aircraft exhaust. They are normally referred to simply as *contrails* and two instances are depicted Figure 3.0.1.

Figure 3.0.1: Thermodynamic contrails from engine exhaust [Reynolds, 2006]. Left: 1981 NOAA photo of a contrail at sunset. Right: Wake vortex causes a corkscrew effect which, when seen from some angles, can appear as puffs along a contrail's length.

[1] A term introduced by British pilots in 1942 as an abbreviation for condensation trails [Schumann, 2002].

3.1 Early history of contrail study[2]

Aircraft reached the altitudes required at midlatitudes for contrail formation between 1914 and 1919. The first publication on observation of contrails ocurred in 1919, citing an observation made in 1915: "*...the condensation of a cumulus stripe from the exhaust gases of an aircraft...*" was visible for a "*long*" time. Documented in 1921, eyewitnesses in 1918 saw "*...unusual clouds that were formed in the wake of airplanes...*". The many reports of strange trails behind high flying aircraft were only marginally interesting at the time. The origin of contrails remained unknown and various causes such as vibration of the engine, electrical charge, propellor turbulence and heat induced cloud convection were discussed: an indication of the state of cloud knowledge at the time.

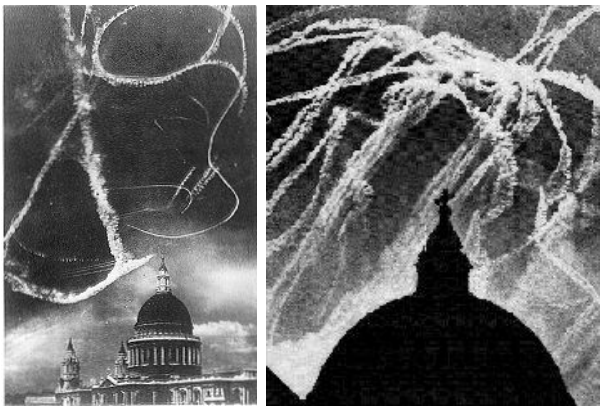

Figure 3.1.1: Dogfights create contrails over St Paul's Cathedral during the Battle of Britain, 1940 [Constable, 2006, Reynolds, 2006].

Several authors had pointed towards the correct explanation by 1921. The possiblity that water vapour emitted from engines burning hydrocarbon fuel caused supersaturation with respect to liquid water, and thereby lead to cloud formation, was initially dismissed because the ambient air was considered too dry for cloud formation. The amount of emitted water was also too small to explain the size of contrails which were sometimes observed. Since a large supersaturation would be required in the absence of sublimation nuclei, many authors proceeded to suggest that aircraft emitted dust and soot. Later calculations showed that water and solution droplets would have to form before ice crystals could grow.

Once the miltary consequences of visible contrail became an issue (see examples of contrails from fighter aircraft in Figure 3.1.1), this stimulated further study and publication: much pioneering work on cirrus and contrails took place during World War II. *In situ* measurements of cirrus cloud were made by the Luftwaffe fighter planes over Germany [Sassen, 2002]. In England, investigations into stratospheric humidity, air temperature and threshold conditions for contrail formation were performed in 1942 by Alan Brewer sitting in a Flying Fortress[3] with a good magnifying glass [Brewer, 1999].

Finally, Schmidt [1941] and Appleman [1953] deduced the thermodynamic theory which produces threshold temperatures for contrail formation as a function of ambient pressure, humidity and the ratio of water and heat released in the plume.

[2]This recounting of contrail study history is largely courtesy of the excellent review paper by Schumann [1996].

[3]Said to be one of the six Flying Fortresses given as a personal gift from Roosevelt to Churchill.

3.2 How contrails form and where they occur

Pure water does not freeze at 273.15 K (0°C): between temperatures of -40°C and 0°C, it continues to exist in a liquid supercooled state, freezing only if nucleation nodes are present. Supercooled pure water droplets do homogeneously freeze rapidly below the threshold temperature of ~ -40°C, and soluble matter is capable of depressing this freezing temperature. At temperatures higher than -40°C, particles in a contrail may thus remain liquid and supercooled, especially if small and free from a substrate capable of causing immersion freezing. Many if not all liquid particles will, however, freeze during the contrail's lifetime: a young contrail has large cooling rates.

Understanding how water vapour transitions to ice is vital if attempts are to be made to model ice clouds formed from persistent contrails. There are two microphysical paths from water vapour to ice [Minnis, 2005, Schumann, 1996]:

- The direct sublimation of water vapour to ice crystals is a transformation which requires a relative humidity well in excess of 100% and a pre-existing nucleus of, or similar to, ice. These nuclei are relatively rare.

- Ice can also occur via two steps:

  - Water vapour forms liquid droplets, which then form ice crystals. For the gas to liquid transition, a relative humidity greater than 100% is required. If a lower water vapour concentration is present, low supersaturation droplet formation can occur if nuclei (typically abundant in the atmosphere) are present.
  - The liquid to solid process also require a relative humidity greater than 100%. If the temperature is then below -40°C then all droplets will freeze instantaneously. A higher temperature requires nuclei: aircraft icing is an example where a very large nucleus for ice formation (the plane itself) is present.

More water vapour (a higher supersaturation) is required to form an ice crystal than to form a water droplet (except at extremely low temperatures). Less water vapour is required to maintain or grow an ice crystal than is required to form a water droplet: ice particles grow much faster than liquid particles from the same available water vapour. Therefore the easiest path towards ice is the formation of water droplets in an area where there are none, after which freezing occurs, followed by the growth of these particles until surrounding excess water vapour is exhausted or the droplet sediments out.

For propellor driven and jet aircraft, contrails are not comprised solely of aviation emissions. Rather, the aircraft exhaust triggers the formation of additional clouds from natural water vapour present in the atmosphere. Contrails form a short distance away from the aircraft, typically 10 to 20 m after the tail. If the temperature of the ambient air is below a certain threshold, liquid saturation may be achieved in the young plume due to the mixing between the warm and moist exhaust and the cooler atmosphere. This changes the humidity, temperature and saturation vapour pressure in the plume's vicinity. If liquid saturation is reached, liquid droplets form by condensation of water vapour mainly on soot and volatile particles in the aircraft exhaust but also on pre-existing nuclei in

the atmosphere. Many liquid droplets subsequently freeze quickly and form ice particles [Sausen et al., 1998, Schumann, 2005, Starr and Quante, 2002].

Saturation with respect to ice (not uncommon in the upper troposphere) is not solely sufficient for contrail formation. Where ice saturation *does* occur, as well as the liquid saturation required for initial formation, persistent contrails develop. These do not evaporate when mixed with the environment and last until their relative humidity drops to below ice saturation. This can occur via mixing with dry air, subsidence, radiative heating or sedimentation into drier air. Conversely, if the ambient air is suitably dry, contrails are short lived.

Generally, a large potential for contrail formation exists in the upper troposphere, particularly in the tropics but also at midlatitudes. More specifically, such situations typically occur ahead of warm fronts in a cyclone or downstream of convective complexes [Sausen et al., 1998]. Persistent contrails have been observed to occur in particular ahead of frontal cirrus bands of warm fronts and at the southern side of jet streams, but occur also in clear air remote from synoptic disturbances. In clear air, the vertical motion needed for adiabatic cooling may be caused by gravity waves. Humid air upon such elevation, reaches ice saturation 300 m before water saturation at $-40°$C [Schumann, 1996]. Figure 3.2.1 shows the likelihood of cirrus formation during aircraft operation.

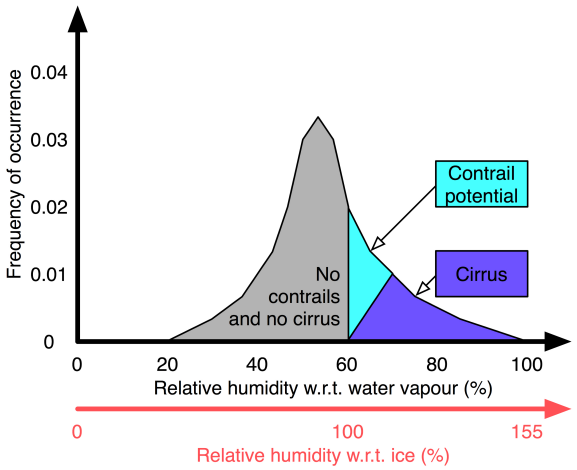

Figure 3.2.1: Probability distribution of relative humidity encountered at cruise altitude ($T < -39°$C), after Minnis [2005]. Ice supersaturation is found 10-20% of the time which corresponds to potential for contrail formation.

Contrails often form near to or within extant cirrus [Minnis, 2005]. Quantifying individual contrail effects is difficult because of continuous air traffic, existing cirrus clouds and poor measurements of humidity fields. Data pertaining to contrails is also scarce: observational global contrail statistics for multi-year periods are not available at present, nor does a climatology for frost saturation exist [Sausen et al., 1998, Schumann, 1996].

The continental United States (frequently referred to as CONUS) and mainland Europe often form the targets of localised contrail studies, the densely trafficked Northern Atlantic less so. Estimates and analyses lead to a contrail coverage figure of 0.4 - 0.5% over Europe with regional maxima of 2% over the North Atlantic flight corridor. Observations of cirrus and contrails from the surface and from satellites show that contrails are consistent with the cirrus trend over the USA, but not over Europe [Minnis, 2005]. These studies do not account for older contrails which grow to large sizes and are no longer linear in shape, nor for "natural" clouds which have evolved from emitted aerosols. The percentages should therefore be taken as lower limits of actual cirrus coverage from contrails [Sausen et al., 1998].

3.3 Contrail theory: the Schmidt-Appleman criterion

The SCHMIDT-APPLEMAN CRITERION is an algorithm which specifies whether a contrail can form in an area based on several local physical parameters (temperature, pressure and humidity) as well as certain attributes of the engine and fuel (aircraft propulsion efficiency, emission index and specific combustion heat). First formulated over fifty years ago by Schmidt [1941] and Appleman [1953], these references remain ubiquitous in the literature surrounding contrails due to continuous validation of the original concept. The thermodynamic theory has been tested extensively from 1941 to the present day via *in situ* observations and measurments behind aircraft. Similarly, the mixing plots and the Schmidt-Appleman diagram used to visualise the thermodynamics have become iconic in contrail papers. An updated version of the criterion with an accompanying Fortran implementation was published more recently by Schumann [1996], which we will here recount. Table 3.3.1 details the required constants and is followed by the derivation.

Constant	Symbol	Value	Units
Specific heat capacity of air	c_p	1004	J kg^{-1} K^{-1}
Ratio of molar masses of water vapour and air	ε	0.622	[None]
Overall propulsion efficiency	η	0.3 to 0.4	[None]
Emission index	$\mathrm{EI}_{\mathrm{H_2O}}$	1.223	kg kg^{-1}
Specific combustion heat	Q	43.2×10^6	J kg^{-1}

Table 3.3.1: Constants used in the Schmidt-Appleman criterion. Values for $\mathrm{EI}_{\mathrm{H_2O}}$, Q and η applicable for modern (2005) aircraft [Schumann, 2005].

Aviation fuel contains molecules primarily consisting of hydrogen and carbon. Burning one mass unit of fuel with $(N-1)$ mass units of air results in N mass units of exhaust gases. N can therefore be referred to as the dilution factor.

For water:

$$\mathrm{EI}_{\mathrm{H_2O}} = Nm_P + (N-1)m_E, \tag{3.3.1}$$

where m is the mass fraction of water, the subscript E refers to the environment and P denotes the plume which forms afterwards. The Emission Index (EI) for water, $\mathrm{EI}_{\mathrm{H_2O}}$, is the number of mass units of water vapour produced per mass unit of fuel combusted in air. We can rearrange the expression for the difference in mass fractions between the plume and the environment:

$$\Delta m = m_P - m_E = \frac{\mathrm{EI}_{\mathrm{H_2O}} - m_E}{N}. \tag{3.3.2}$$

The engine also releases heat Q per unit mass of fuel burnt in air. A fraction of the heat η (also known as propulsion efficiency[4]) is converted to work, propelling the aircraft.

[4] $\eta = \frac{FV}{Q\frac{\mathrm{dm_F}}{\mathrm{dt}}}$, where FV is the work rate (thrust times true air speed), and $Q\frac{\mathrm{dm_F}}{\mathrm{dt}}$ is the chemical energy (specific combustion heat times rate of fuel mass flow). The value of η at cruise altitudes was close to 0.2 in the 1950s, near 0.3 on average for the subsonic airliner fleet in 1992 and may reach 0.5 for new engines built after 2010 [Schumann, 1996, 2005]. Currently, it lies between 0.3 and 0.4, as in Table 3.3.1. Contrail coverage is strongly sensitive to flight altitude and weakly sensitive to propulsion efficiency η [Sausen et al., 1998].

Ignoring heat losses due to incomplete combustion and assuming that heat and water mix with the plume quickly:

$$Q_{\text{total}} = \eta Q_{\text{work}} + (1-\eta)Q_{E,P}, \tag{3.3.3}$$

where the first term is heat "lost" to the work and the second term is the heat expelled per unit mass of fuel (to be partitioned between the environment E and the plume P). This second term can thus be written:

$$(1-\eta)Q_{E,P} = Nh_P + (N-1)h_E, \tag{3.3.4}$$

where h is the heat content or enthalpy. This leads to:

$$\Delta h = h_P - h_E = \frac{(1-\eta)Q_{E,P} - h_E}{N}. \tag{3.3.5}$$

The dilution factor N increases without limit during mixing of the plume with the environment, and Equations 3.3.2 and 3.3.5 are only satisfied for all values of N under adiabatic and isobaric conditions. Since ambient heat and mass fraction of H_2O are small compared to $\text{EI}_{\text{H}_2\text{O}}$:

$$\Delta m \simeq \frac{\text{EI}_{\text{H}_2\text{O}}}{N}, \tag{3.3.6}$$

$$\Delta h \simeq \frac{(1-\eta)Q_{E,P}}{N}. \tag{3.3.7}$$

$\text{EI}_{\text{H}_2\text{O}}$ and $(1-\eta)Q_{E,P}$ are constants so a h-m plot would show $h_P(m_P)$ as a straight line.

For ideal gases, the specific enthalpy is a pure function of temperature, T:

$$h - h_E = \int_{T_E}^{T} c_p \,\mathrm{dT}, \tag{3.3.8}$$

where $c_p = c_p(T)$, the specific heat at constant pressure.

The specific heat c_p also depends on the composition of the exhaust gases, where small ambient water content (m_E) and non-air exhaust components can be neglected for large dilution (N). The value of c_p varies by $\sim$50 J kg^{-1} K^{-1} between 200 and 600 K (the typical temperature of the core exhaust) for dry air. Only for large dilution N and when the plume temperature T_P has dropped below 50°C (323.15 K) can a constant value of $c_p \simeq 1004$ J kg^{-1} K^{-1} be used. Assuming this is so and setting $h = h_P$ and $T = T_P$:

$$\begin{aligned} h_P - h_E = \int_{T_E}^{T_P} c_p \,\mathrm{dT} &\simeq c_p(T_P - T_E) \\ \Rightarrow \frac{\Delta h}{\Delta T} &= c_p. \end{aligned} \tag{3.3.9}$$

Substituting for Δh from Equation 3.3.7:

$$\begin{aligned} c_p &= \frac{(1-\eta)Q_{E,P}}{N\Delta T} \\ \Rightarrow \Delta T &= \frac{(1-\eta)Q_{E,P}}{Nc_p}. \end{aligned} \tag{3.3.10}$$

Water concentration m is related to the partial pressure of H_2O e by:

$$m = \frac{R_{\text{air}}}{R_{\text{H}_2\text{O}}} \frac{e}{p} = \varepsilon \frac{e}{p}, \tag{3.3.11}$$

where p is the total air pressure and $\varepsilon = 0.622$. Therefore

$$e_p = \frac{p}{\varepsilon} m_P \qquad , \qquad e_E = \frac{p}{\varepsilon} m_E. \tag{3.3.12}$$

If we define:

$$G = \frac{\Delta e}{\Delta T} = \frac{e_P - e_E}{T_P - T_E}, \tag{3.3.13}$$

and take Δe from Equation 3.3.13 and ΔT from Equation 3.3.10, we have:

$$G = \frac{\frac{p}{\varepsilon} \Delta m}{\frac{(1-\eta) Q_{E,\,P}}{N c_p}}, \tag{3.3.14}$$

which, by Equation 3.3.6, is:

$$G = \frac{\frac{p}{\varepsilon} \frac{\text{EI}_{\text{H}_2\text{O}}}{N}}{\frac{(1-\eta) Q_{E,\,P}}{N c_p}} = \frac{p c_p \text{EI}_{\text{H}_2\text{O}}}{\varepsilon (1-\eta) Q_{E,\,P}}, \tag{3.3.15}$$

an important parameter.

Figure 3.3.1, the mixing plot and Figure 3.3.2, the Schmidt-Appleman diagram, encapsulate the thermodynamics visually.

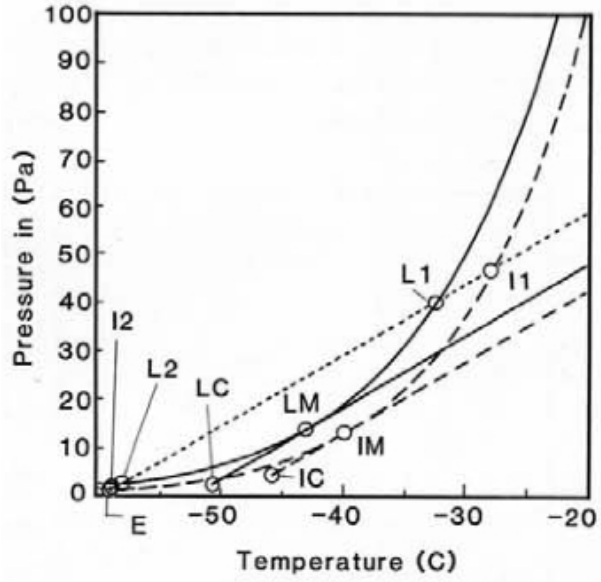

Figure 3.3.1: A water vapour partial pressure versus temperature plot. At point of exit from the engine (the temporal origin of the mixing line), the conditions are on the far upper right hand corner, outside of the range plotted. Each dot corresponds to a specific value of N, which increases with time. Progressive dilution and mixing leads to a decrease of pressure and temperature, causing the mixing lines to eventually arrive, travelling leftwards and downwards with increasing time, inside the range shown. Annotations are explained in the text.

For sufficiently low temperatures (so that $c_p \neq c_p(T)$) and without a phase change, an e_P-T diagram representing mixing would show a straight line (of gradient G) for isobaric mixing (Figure 3.3.1).

Curved lines are saturation pressures for plane surfaces of:

Dashed: Liquid water, represented by the function e_L.

Solid: Ice, function e_I.

Straight lines represent isobaric mixing, for contrail onset at:

Dashed: Ice saturation.

Solid: Liquid water saturation.

Dotted: Ambient temperature.

G is constant for mixing lines, therefore it can be seen that the mixing lines may cross the liquid saturation curve if the temperature is below the threshold temperature, T_{LC}. $T_E = T_{LC}$ (the end point of the mixing line) at threshold conditions, where the mixing line just touches the liquid saturation curve e_L at T_{LM}. At that point,

$$\frac{\mathrm{d[e_L]_{LM}}}{\mathrm{dT}} = G. \tag{3.3.16}$$

T_{LC} can be related to T_{LM} by making use of G:

$$\begin{aligned} \frac{[e_L]_{LM} - [e_L]_{LC}}{T_{LM} - T_{LC}} &= G \\ \Rightarrow T_{LC} &= T_{LM} - \frac{[e_L]_{LM} - [e_L]_{LC}}{G}. \end{aligned} \tag{3.3.17}$$

Since the end point of the mixing line is at environmental temperature T_E and water vapour partial pressure e_E, we correspondingly have:

$$T_E = T_{LM} - \frac{[e_L]_{LM} - [e_L]_E}{G} \tag{3.3.18}$$

If, for threshold conditions, the partial pressure of the environment e_E is such that (Equation 3.3.13):

$$[e_L]_E = U[e_L]_{LC}, \tag{3.3.19}$$

U being relative ambient humidity, then substituting in to Equation 3.3.18, we have:

$$T_E = T_{LM} - \frac{[e_L]_{LM} - U[e_L]_{LC}}{G}. \tag{3.3.20}$$

Since $T_E = T_{LC}$ at threshold conditions, we arrive at:

$$T_{LC} = T_{LM} - \frac{[e_L]_{LM} - U[e_L]_{LC}}{G}. \tag{3.3.21}$$

A similar treatment for the ice saturation case yields:

$$T_{IC} = T_{IM} - \frac{[e_I]_{IM} - U[e_L]_{IC}}{G}. \tag{3.3.22}$$

These implicit equations (3.3.20 and 3.3.21) require iteration in order to output the threshold temperature T_{LC} for a given relative humidity U. Figure 3.3.2 comprises T_{LC} lines as a function of altitude with the atmosphere superimposed. This is known as a Schmidt-Appleman diagram.

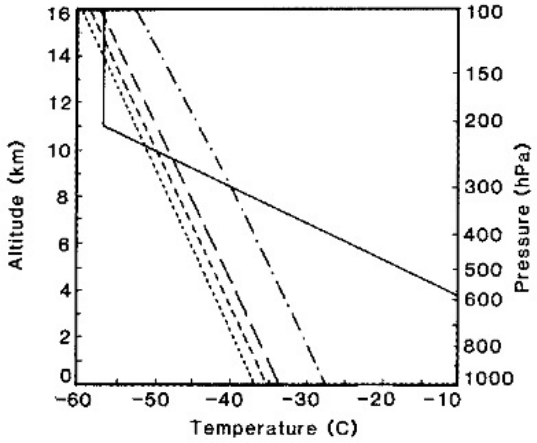

Figure 3.3.2: A SCHMIDT-APPLEMAN DIAGRAM. The solid line is the international standard atmosphere. Dashed lines are threshold temperatures for kerosene fuel and propulsion efficiency of 0.3. From left to right, the lines are for 0, 30, 60 and 100% relative humidity.

3.3.1 Schmidt-Appleman theory summary

A mixing diagram is shown in Figure 3.3.3 with exaggerated features and annotations. It is clear that in order to form contrails, the plume has to undergo supersaturation with respect to liquid water. For fixed engine and fuel parameters (propulsion efficiency, emission index and specific combustion heat), the gradient to the mixing line remains constant, as for all mixing lines in Figure 3.3.3. The differing locations of the endpoints of the mixing lines (arrow heads) are indicative of the variety of ambient conditions eventually encountered by the mixture of environmental and plume gases and particles. Only sufficiently low temperatures can lead to persistent contrails.

Atmospheric temperature has a lapse rate ($\sim$6.5 °C km^{-1}) as far as the tropopause. This is represented by the red line on the exaggerated Schmidt-Appleman diagram (Figure 3.3.4). For a constant value of humidity U, the threshold temperature for contrail formation T_{LC} is inversely proportional to pressure (green line). If atmospheric temperature at a specific altitude (red line) is lower than the threshold temperature for contrail formation at that altitude (green line), then contrails can form. The only place this occurs is shaded in blue in Figure 3.3.4 for the example relative humidity used.

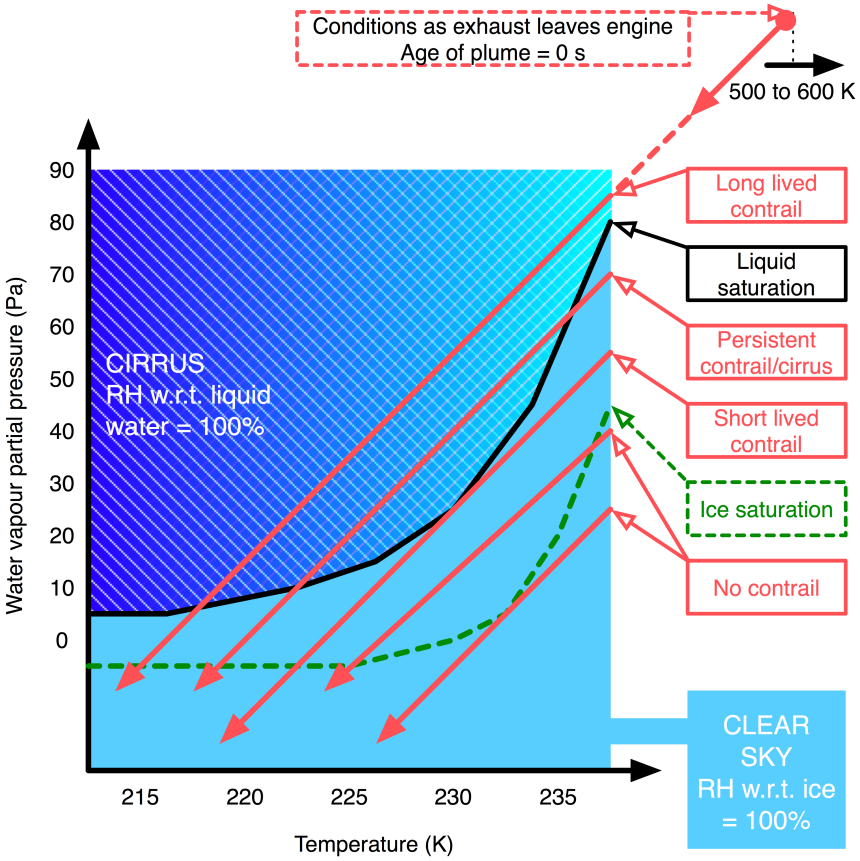

Figure 3.3.3: If ($T > -39°$C then the mixing line which would cross the liquid saturation region would be very steep. Contrails are therefore formed more easily at lower temperatures [Minnis, 2005].

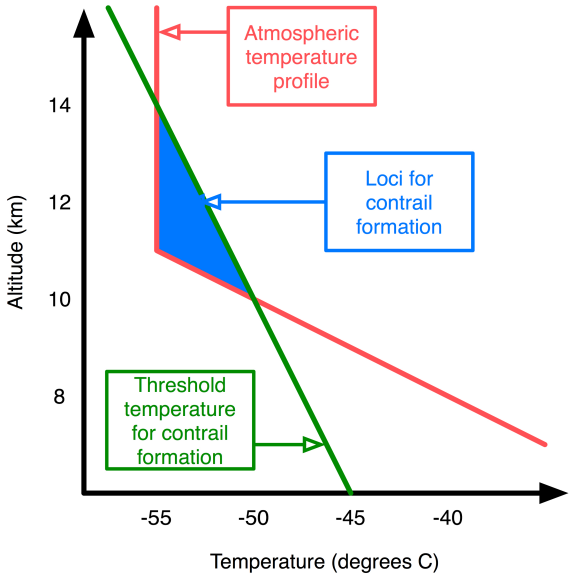

Figure 3.3.4: $U = 0$. Contrails can only form in the triangle bounded by the T_{LC} and atmosphere lines.

	Aircraft engine nozzle	Exhaust emission	Interaction between plume and atmosphere	Contrail	Persistent contrail				Cirrus
Age (s)	0	0 - 0.01	0.01 - 0.1	0.1 - 1	1 - 10	10 - 100	100 - 1000	1000 - 10^5 to 10^6	> 10^5 to 10^6
Temp. (K)	> 500 to 600	500 to 600 (plume temperature)	400 - 300	300 - 250	250 - [ambient]				[Ambient]
Width (m)	0	< 1			1 - 1,000			100,000	
Exhaust dynamics	Jet regime Exhaust material in entrained in counter rotating vertices				Vortex regime Vortices propagate downwards		Dissipation/ dispersion regime Buoyancy effect dominates	Diffusion regime Shear and synoptic wind dominates	["Natural" cloud dynamics]
Micro-physics & chemistry	Sulphur (SO_2, H_2SO_4, etc.)	Oxidation of sulphur species Binary homogeneous nucleation of H_2SO_4 & H_2O			Growth of particles by condensation Growth of particles by coagulation				
	Soot, metal	Binary heterogeneous nucleation of H_2SO_4 & H_2O on soot and metal							
	H_2O vapour	Freezing of H_2SO_4-H_2O aerosol Liquid H_2O saturation reached within plume			Evaporation, scavenging and freezing affect particles Ambient ice supersaturation				
Data set	[None]	Flight paths TRADEOFF inventory	Global temperature, pressure & humidity ECMWF ERA40						Cirrus cloud climatologies GRAPE, ISCCP, HIRS, MIPAS, etc.
Pertinent algorithm		Schmidt-Appleman criterion						Aerosol & ice microphysics	
Module		Contrail formation model						The new SAMM	

Table 3.3.2: Emission evolution until cirrus formation. Compiled from Penner et al. [1999], Karcher [1995] and Paugam et al. [2006].

Chapter 4

Research and results to date

4.1 Method

The evolution of aircraft emissions into eventual cirrus cloud spans many different processes. Table 3.3.2 shows the order and the temporal, spatial and temperature scales of each process. Modelling the life cycle of aircraft exhaust, from emissions to contrail cirrus formation will need to simulate the main processes from the *Microphysics & chemistry* and *Exhaust dynamics* sections in Table 3.3.2. The focus of the project is on developing a microphysical model, thus certain assumptions will need to replace plume dynamics. This is considered appropriate since the Schmidt-Appleman criterion requires no information about winds, turbulence, etc. in order to predict contrail occurrence, and because there also exists considerable uncertainty about the number and nature of particles which survive from the emissions to the contrail phase. A detailed chart of the planned models is shown in Figure 4.1.1, which can be taken as a template for which processes will be included from Table 3.3.2 and pursued over the course of the project.

Three models are shown in Figure 4.1.1 between which all proposed tasks are assigned. On the left is a contrail model, the top right, a microphysical model and the bottom right, a cirrus comparison model. The goal of this separation is to have an initial contrail model (§4.4) which designates those areas on the globe in which contrails can form. Only in the locations thus designated as potentially contrail-bearing will a second model (§4.5) operate. This latter model will simulate the microphysical changes undergone by liquid and solid particles resulting from emissions.

This proposed method does not imply that the models run in chronological fashion, or that the results from one are fed into the other as its sole direct input. Rather, the microphysical model is actually responsible for the complete life cycle of aircraft exhaust, from the gas phase to the eventual cloud formed of ice crystals. The purpose of the contrail model is to conserve time such that the microphysical model is not run indiscriminately in places where contrails or cirrus cannot occur. Finally, the cirrus comparison model (§4.3) will evaluate the degree of discernibility between the contrail cirrus predicted by the microphysical and global cirrus climatologies. Its role is to validate the microphysical model and establish if the modelled contrail cirrus signature is significant.

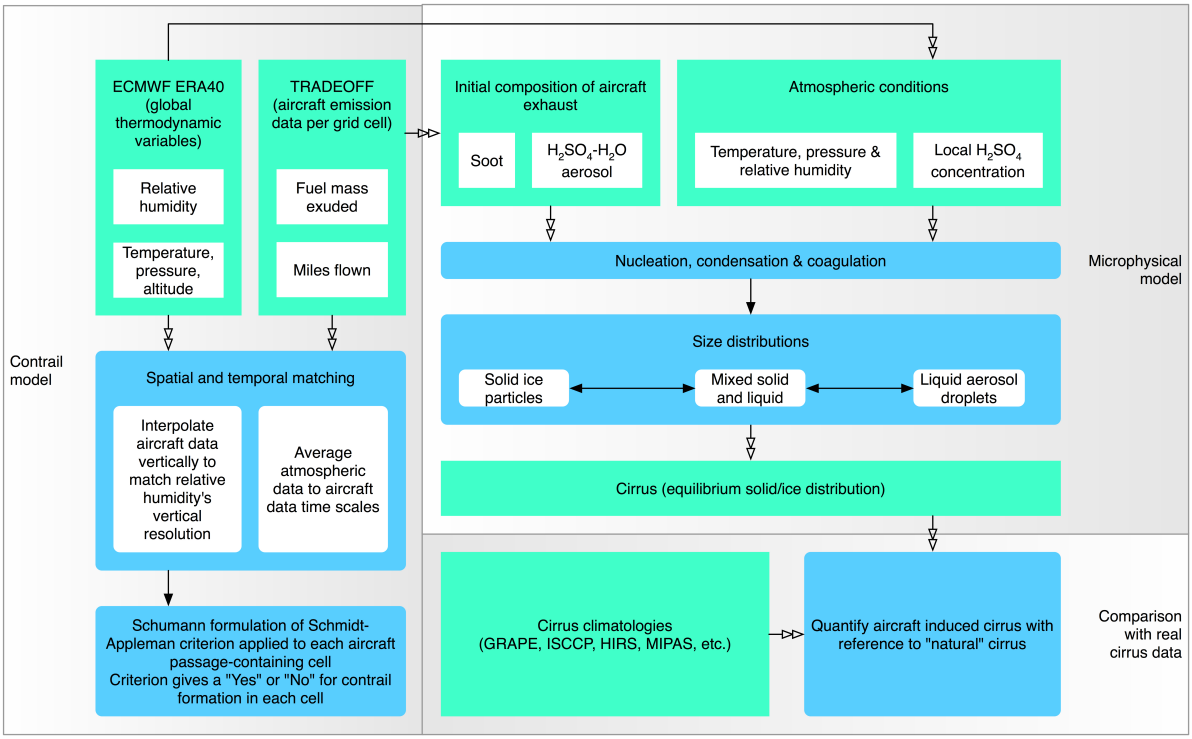

Figure 4.1.1: Three proposed models to produce global maps of aircraft-induced cirrus.

4.2 Initialisation data

The first task was to create a single data set spanning the globe where every cell will have the necessary input data for checking viability of contrail formation and initialising the microphysical model. **E**CMWF **40** year **r**e-**a**nalysis (ERA40) data sets were used for atmospheric parameters and TRADEOFF for scheduled flight path information (Figure 4.1.1). TRADEOFF data (resolution is 1° by 1° by $\sim$ 600 m) over January 2003 are displayed in Figure 4.2.1, where the heavy aviation traffic over the North Atlantic and Japan is clearly visible.

ERA40 data are also at horizontal resolution of 1° by 1°, but the vertical spacing depends on pressure levels or model levels, which follow the terrain near the ground. Since relative humidity cannot be vertically interpolated without introducing serious errors into the humidity data [Gierens, 2006b, Lee, 2005, Lim, 2005], the other quantities (pressure, temperature, miles flown and mass of fuel exuded) were interpolated to the relative humidity data set's dimensions. The result was a final data set comprising all the necessary parameters for the Stratospheric Aerosol Microphysical Model (SAMM) and the contrail model.

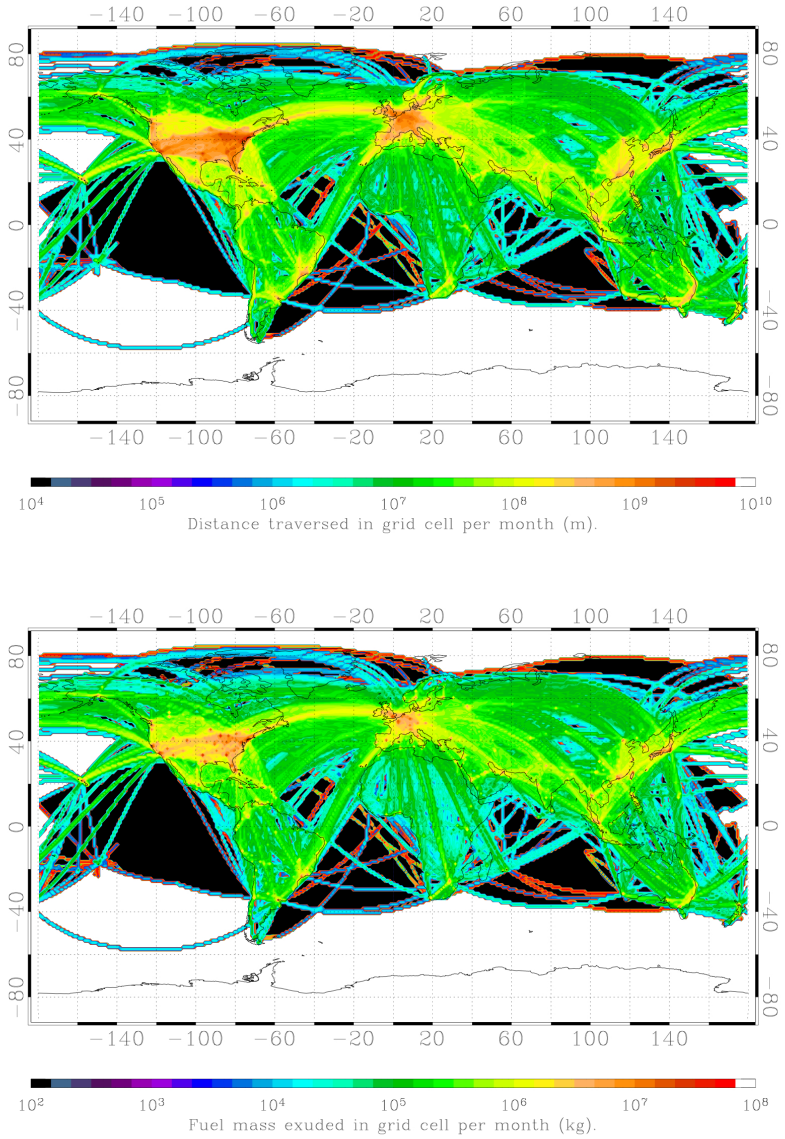

Figure 4.2.1: Great circle routes of scheduled flights. Private and non-scheduled flights are not included. These data are integrated over altitude. Top: Distance flown per grid cell. Bottom: Fuel mass emitted in each grid cell.

4.3 Cirrus comparison model

Global cirrus coverage can be ascertained from established cloud climatologies such as the High resolution Infrared Radiation Sounder (HIRS) or ISCCP. In preparation for comparison of results from contrail cirrus modelling to cirrus climatologies, cirrus cloud amount (measured in percentage cover) from these climatologies have been plotted. Figure 4.3.1 is cirrus from HIRS.

The cirrus description from Figure 2.3.1 was used by ISCCP to produce the climatology in Figure 4.3.2. The ISCCP cirrus climatology shows several artifacts and the high reflectivity from the northern summer is responsible for missing data at the top

of the plot. Lim et al. [2006] therefore ignored data at latitudes $> 45°$ and $< 45°$ when making use of the climatology for calculations on cirrus coverage. Despite the aberrations, there is a high degree of correlation for cirrus detected between the HIRS and ISCCP climatologies. Highs exist in both over South America, central Africa and especially over the Pacific/Indonesia region.

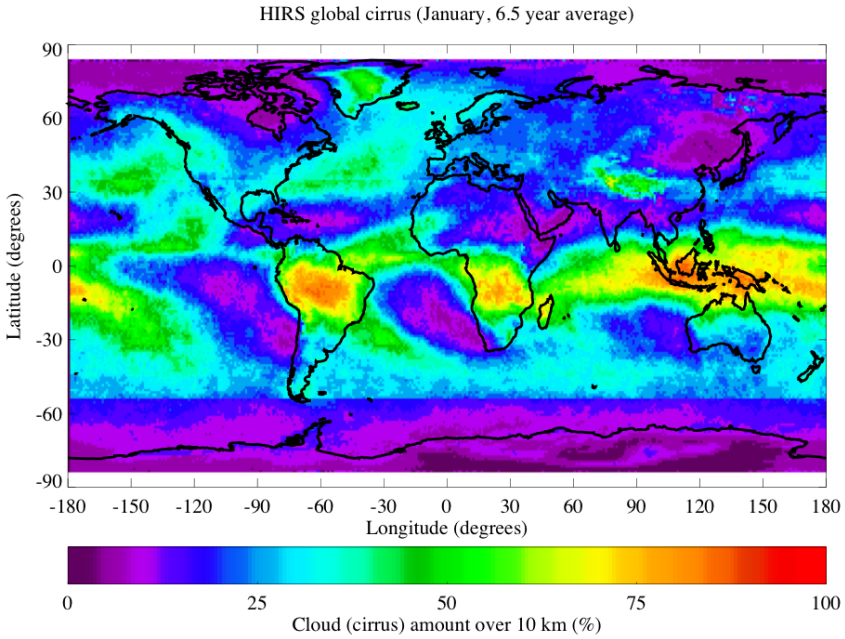

Figure 4.3.1: HIRS global cirrus, horizontal resolution is 2.5° by 2.5°.

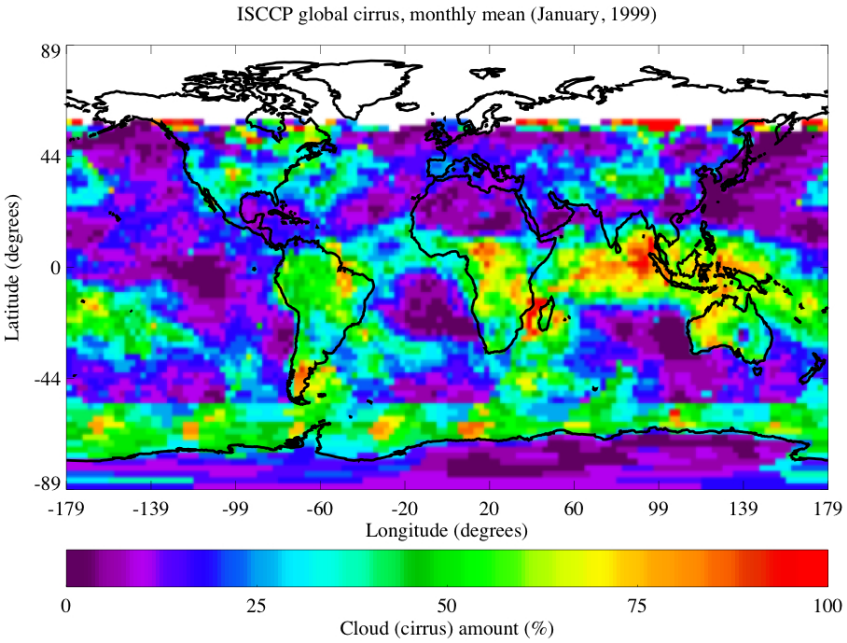

Figure 4.3.2: Cloud climatology from ISCCP, January 1999. Horizontal reolution is 2.5° latitudinally with equal area longitudinally.

4.4 Contrail model

A model capable of predicting contrail presence has been developed. It's aim is to ascertain whether ambient conditions are suitable for persistent contrail formation. Where a non-zero number of miles are flown in a grid box, the contrail model flags the cell as either contrail-bearing or unsuitable for contrail formation by applying the Schmidt-Appleman criterion, as reviewed by Schumann [1996] (see §3.3.1). The critical input parameter is relative humidity (as well as temperature and pressure), which is derived from ERA40 data for the same period as the TRADEOFF flight path information (January, 2003).

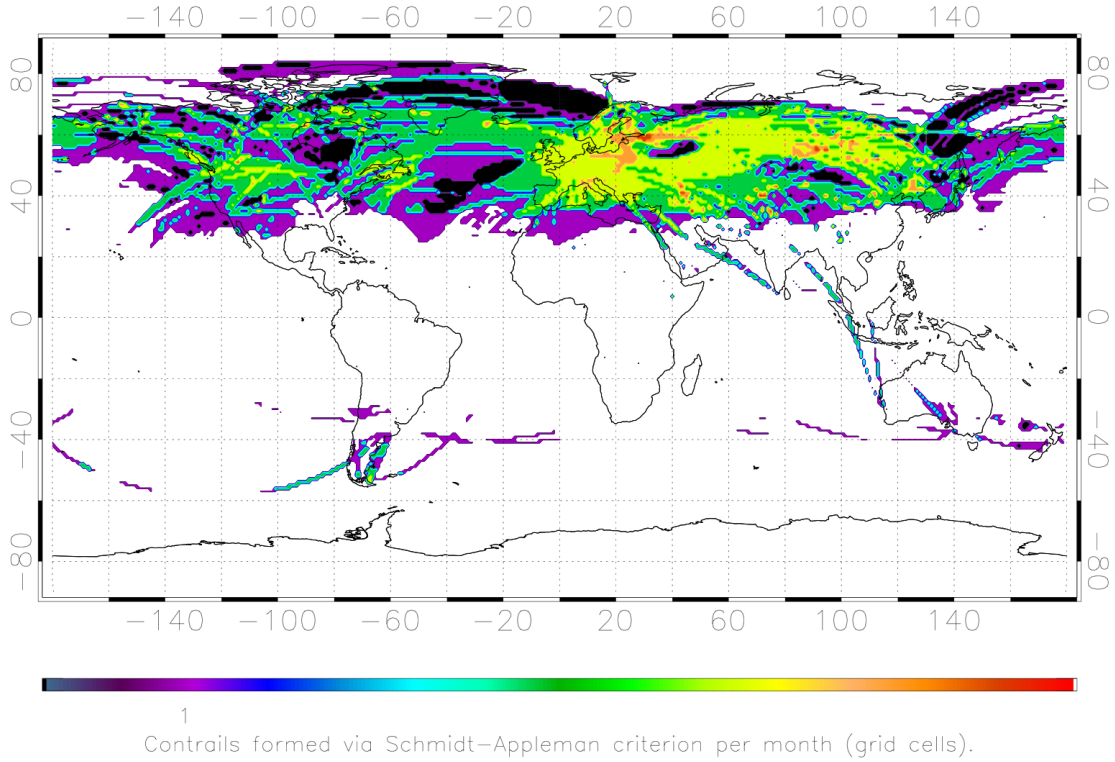

Figure 4.4.1: Number of grid cells for which contrails form, over January 2003. Each cell is 1° by 1° (this plot vertically integrated over all height levels).

The upper limit for global contrail coverage is an assumption that everywhere aircraft fly, contrails form. This corresponds to contrail occurence matching the flight paths in Figure 4.2.1. Since the Schmidt-Appleman criterion will obviously find many locations too warm or dry for contrail ocurrence, global contrail coverage will be a subset of the maximum. Running the contrail model applied the Schmidt-Appleman criterion to every grid cell through which flight occurred (Figure 4.2.1) and the cells flagged as contrail-bearing are shown in Figure 4.4.1 (integrated vertically as in Figure 4.2.1).

Figure 4.4.1 shows some interesting features when compared to Figure 4.2.1:

- Contrails form predominantly in the northern hemisphere.

- The areas of densest air traffic do not correspond to where the most contrails form. Europe, the United States and Japan are the most trafficked destinations, yet contrail density is highest over North-east Europe and North-west Asia.

- The tropics see nearly no contrail formation.

Contrail formation preference for the north cannot be attributed to the higher frequency of flight in that hemisphere (Figure 4.2.1) since the contrail model does not yet use the number of miles flown or fuel mass exuded for any of its calculations. Instead, this is due to the Schmidt-Appleman criterion: contrails form preferentially at lower atmospheric temperatures and the plot is showing a northern winter. It is for the same reason that the tropics see almost no contrail formation: the tropopause is much higher (at ∼17 km), therefore it is warmer at cruise altitudes, even in the northern hemisphere's tropics.

4.5 Microphysics

A Stratospheric Aerosol Microphysical Model (SAMM) has been developed by Tripathi et al. [2004] at the University of Oxford. It requires ambient physical paramaters to simulate nucleation, condensation of H_2SO_4 and H_2O on to droplets and coagulation of H_2SO_4-H_2O liquid droplets (Figure 4.5.1). An aerosol size distribution (with particle mass doubling per subsequent bin) can then be produced along with total surface area density and H_2SO_4 weight fraction for each droplet size.

A parameterisation by Vehkamaki et al. [2002] provides a nucleation rate[1] of H_2SO_4-H_2O aerosol particles with a computing time enhancement factor of 500 over non-parameterised nucleation rate calculations, with a validity range of 190.15 to 305.15 K [Tripathi et al., 2004]. Condensation makes use of non-iterative processes developed by Jacobson [1997, 1999, 2002] to solve growth equations and implement mass conservation. Activities are taken from Zeleznik [1991]. A semi-implicit computationally fast scheme by Jacobson et al. [1994] allowed construction of a Brownian coagulation kernel. Results

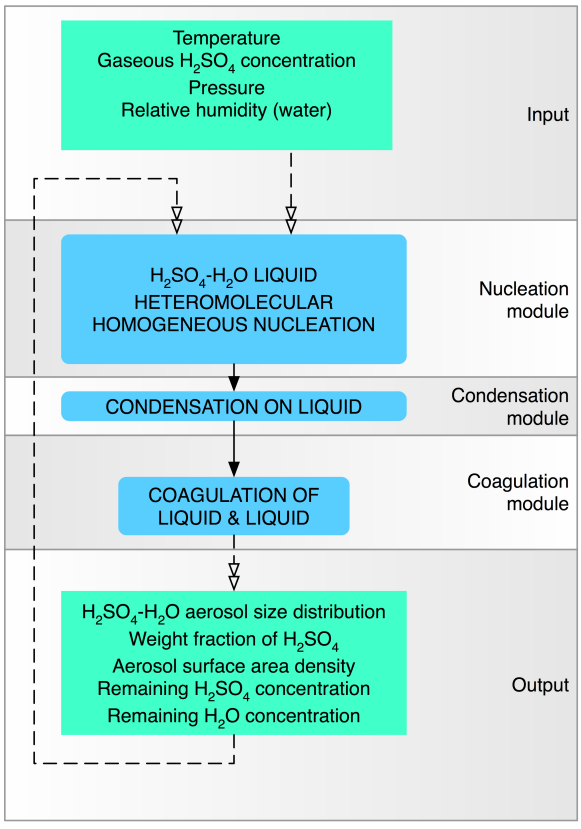

Figure 4.5.1: Chart of SAMM's operation and parts.

[1] Generally referred to as J with units of new particles formed per unit time per unit volume.

from the coagulation kernel were found to approach Smoluchowski's (exact) analytical solution for coagulation [Jacobson et al., 1994, Tripathi et al., 2004].

The result of these implementations is that SAMM can produce an evolving aerosol size distribution (over a discrete time step of half an hour) at a much faster rate than iterative numerical methods for nucleation, condensation and sedimentation.

SAMM is only capable of simulating liquid aerosol and does this by creating a single size distribution of liquid H_2SO_4-H_2O particles from initial concentrations of water vapour and gaseous sulphuric acid. Cirrus is characterised by ice. The creation of solid particles and their subsequent interactions with other solid particles and liquid droplets therefore need to be added to allow cirrus ice particle growth. Figure 4.5.2 is a schematic of the proposed SAMM with envisaged changes.

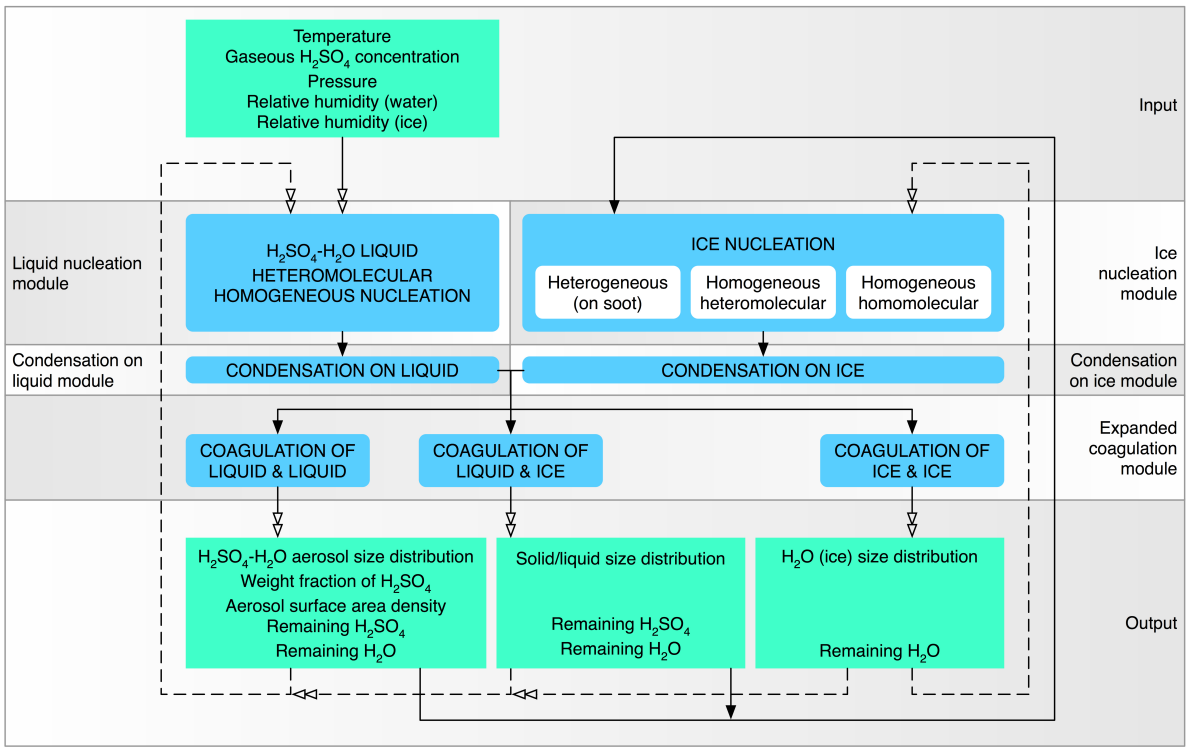

Figure 4.5.2: Design of the new SAMM. Compare to Figure 4.5.1: two entirely new modules are required (ice nucleation, condensation on ice) whilst others parts will have to be generalised for operation on more than one size distribution (coagulation, input and output).

Thus far, schemes have been investigated for homomolecular homogeneous and heteromolecular homogeneous ice nucleation, and have been integrated into the nucleation module in SAMM. Koop et al. [2000] has developed a parameterisation for nucleation of pure H_2O (Appendix A.1) requiring only local temperature (valid for 170 to 245 K) and the activity of water for the droplet size being considered (valid for activities ranging between 0.7 and 1.0). This method gives the contribution of homomolecular homogeneous freezing to the total ice nucleation rate.

Modelling, laboratory and field studies show that H_2SO_4-H_2O aerosols can remain supercooled to very low temperatures. Pure water remains liquid only to -40°C, whilst cirrus clouds usually nucleate at temperatures ranging from -80°C to -40°C, depending

on relative humidity. When ice saturation is reached in the atmosphere, nucleation of ice particles is thus most likely on aqueous solution droplets. Therefore critical ice nucleation parameters in aqueous H_2SO_4 droplets rather than those derived from pure water experiments need to be used. Classical nucleation theory along with such data has led to such a parameterisation algorithm for ice nucleation from an aqueous H_2SO_4 droplet (homogeneous heteromolecular ice nucleation) by Tabazadeh et al. [1997, 2000]. Inputs are droplet volume, partial pressure of H_2O and temperature and a full description can be found in Appendix A.2. This method produces the ice nucleation rate for heteromolecular homogeneous freezing and it is particularly applicable to the aerosol that SAMM currently models (H_2SO_4-H_2O).

Both parameterisations output the number of ice particles nucleating per unit volume per unit time, for each size bin in the distribution. Particles which have frozen are then removed from the liquid H_2SO_4-H_2O size distribution to be added to a solid ice distribution.

Chapter 5

Future direction

5.1 Initialisation data

The project should take advantage of the best possible (i.e., most modern) aviation inventory and it should also make use of the most suitable meteorological data on atmospheric conditions.

The currently used TRADEOFF flight data are now over ten years out of date and have recently been superceded by AERO2k[1] sets [Eyers et al., 2004, Lee, 2005]. These contain a more comprehensive inventory of flight paths, relying on real locations of flight paths rather than assuming great circle paths for scheduled aircraft, which is the case for TRADEOFF. They also have more data on emissions per unit length of flight. These new files (publicly available) will be adopted for use, allowing contrail modelling to more accurately reflect global aircraft coverage.

Colleagues involved in aircraft emissions research [Lee, 2005, Lim, 2005] are currently developing a model for contrail coverage based on Sausen et al. [1998] using atmospheric parameters from the National Centers for Environmental Prediction (NCEP). Successful collaboration and comparison of results between efforts can only occur for identical inputs for the Schmidt-Appleman criterion. Thus, a migration from the current ERA40 sets to NCEP data will occur, although ERA40 data will continue to be used for testing the contrail and microphysical models. Parameters from ERA40 data will also use an updated extraction method which will output all atmospheric data on homogenised vertical levels. Currently, all parameters have to be interpolated to relative humidity's vertical resolution and the newer method will reduce the need for interpolation and the attendant degradation of data accruacy.

5.2 Cirrus comparison model

Since progress on the comparison model has thus far been limited to producing cirrus climatologies, significant work needs to be done in order to produce a version which will quantifiably compare modelled contrail cirrus to real cirrus.

Global cirrus coverage can be acquired from other sources apart from the current reliance on ISCCP and HIRS. New climatologies which are being actively worked

[1] Not an acronym.

on include Global Retrieval of ATSR cloud Parameters and Evaluation (GRAPE) and Michelson Interferometer for Passive Atmospheric Sounding (MIPAS). An ice cloud climatology can also be modelled from atmospheric conditions [Lim et al., 2006], providing a further alternative.

Global cirrus coverage is estimated at 35% [Tabazadeh et al., 1997] and if the error in this figure as calculated from climatologies is comparable to the contrail cirrus amount, then quantifying anthropogenic contributions to the cirrus trend may prove difficult. A knowledge of the errors and uncertainties in real or modelled cirrus climatologies is therefore essential and will have to be investigated.

While testing the models will be essential throughout the design hurdles presented, it will be the comparison model which will validate contrail cirrus modelling quantifiably and thus establish the contribution of antrhopogenic cirrus to cirrus trends. An algorithm therefore needs to be designed which can assign contrail cirrus a fraction from the total cirrus coverage.

5.3 Contrail model

The main tasks remaining in the contrail model are:

- Contrail cover must be quantified so a meaningful relation can be established between simulated contrail cirrus and natural cirrus.
- The output from the contrail model must be configured to act as in input for the improved microphysical model.

The model description by Sausen et al. [1998] used the Schmidt-Appleman criterion by Schumann [1996] to calculate the coverage of contrails formed from contrails, giving a figure comparable to Cloud Amount (CA) in percentage cover. This work has already been replicated at MMU [Lim, 2005, Lim et al., 2006] and is in contrast to the author's own work which directly uses the formulation by Schumann [1996]. The description by Schumann [1996] only furnishes an affirmative if suitable conditions for contrail formation from emissions exist, not CA. A move towards the method established by Sausen et al. [1998] is therefore highly desirable since it offers a route for comparing model outputs with cirrus climatologies and would also be indicative of contrail spreading after formation. This might well aid in establishing approximations to contrail dynamics which are not otherwise explicit in SAMM.

Finally, the results of the contrail model (latitude, longitude and altitude of where contrails can form along with data on fuel mass, soot, sulphur compounds, etc.) need to be coupled as inputs for the microphysical model. Conditions for ice evolution can thus be initialised consistently for aviation-perturbed regions.

5.4 Microphysics

Three types of nucleation are required in SAMM for ice particle (i.e., cirrus) formation:

- Homogeneous nucleation. This can occur in two ways:

  - HOMOMOLECULAR HOMOGENEOUS nucleation. Theoretically the simplest, this consists of ice forming around an H_2O core.
  - HETEROMOLECULAR HOMOGENEOUS nucleation. Often referred to as BINARY homogeneous nucleation for H_2SO_4-H_2O aerosol, the core contains two molecular species. In this case, they are sulphuric acid and water.

- HETEROGENEOUS nucleation. This is where the daughter particles nucleate on a core which is of an entirely different composition and/or structure. Specifically for aircraft exhaust, the nucleation core tends to be solid and insoluble (mainly soot[2]).

Whilst the parameterisation by Koop et al. [2000] for pure H_2O parameterisation has been successfully coded and tested, simulated nucleation rates of pure ice-on-ice remain negligible. This may be due to either to the initialised atmospheric conditions being unsuitable for non-negligible homogeneous homomolecular ice nucleation, or because the activity of water [Zeleznik, 1991] passed to the nucleation routine (which does not calculate it natively) is outside the limits of the parameterisation. The parameterisation therefore needs to be checked before its contribution towards the ice nucleation rate can be accepted.

Thus far, all (solid) nucleation is approximated almost wholly by heteromolecular homogeneous nucleation and homomolecular, a state of affairs which will need to change if consistent modelling of ice particle formation is to occur. Soot, a blanket term for non-metal solid particles in the exhaust, is also reponsible for liquid particle nucleation in the aircraft plumes. Despite soot's natural hydrophobicity, a coating of H_2SO_4-H_2O aerosol or water reverses this and makes soot hydrophilic and soot's irregular surface may also amplify nucleation [Karcher, 1999]. Soot-nucleated liquid particles therefore also need to be considered for freezing, which means soot concentration, nucleation rate from soot and size distribution produced by soot-induced nucleation need to be characterised.

A heterogeneous nucleation scheme is therefore required for explicitly calculating ice formed under the influence of ejected soot. Candidates include parameterisations by Karcher and Lohmann [2003] (specific to soot with H_2SO_4-H_2O coatings) and Liu and Penner [2005] (more general, deals with both homogeneous and heterogeneous nucleation). Further investigation of one or both of these parameterisations is highly desirable to fill the gaps in the current nucleation regime and to make SAMM capable of simulating the main nucleation processes known to occur in contrails.

Coagulation in SAMM occurs only between particles of a single distribution. By adding more size distributions (liquid, liquid-solid and solid as in Figure 4.5.2), particles in different designated distributions should also coagulate. The coagulation module in SAMM will have to be rewritten in a more generalised format, following Jacobson et al. [1994]. Similarly, condensation in SAMM will have to be expanded to allow condensation on any type of distribution [Jacobson, 2002]. These two improvements will allow SAMM to simulate growth for the nucleated ice particles.

Figure 5.4.1 outlines the pending improvements necessary before SAMM can become fully capable of ice particle evoution.

[2]Metal particles are also present in plumes from corrosion of the engine or trace amounts in aircraft fuel. The role of these as contrail forming agents is comparatively low.

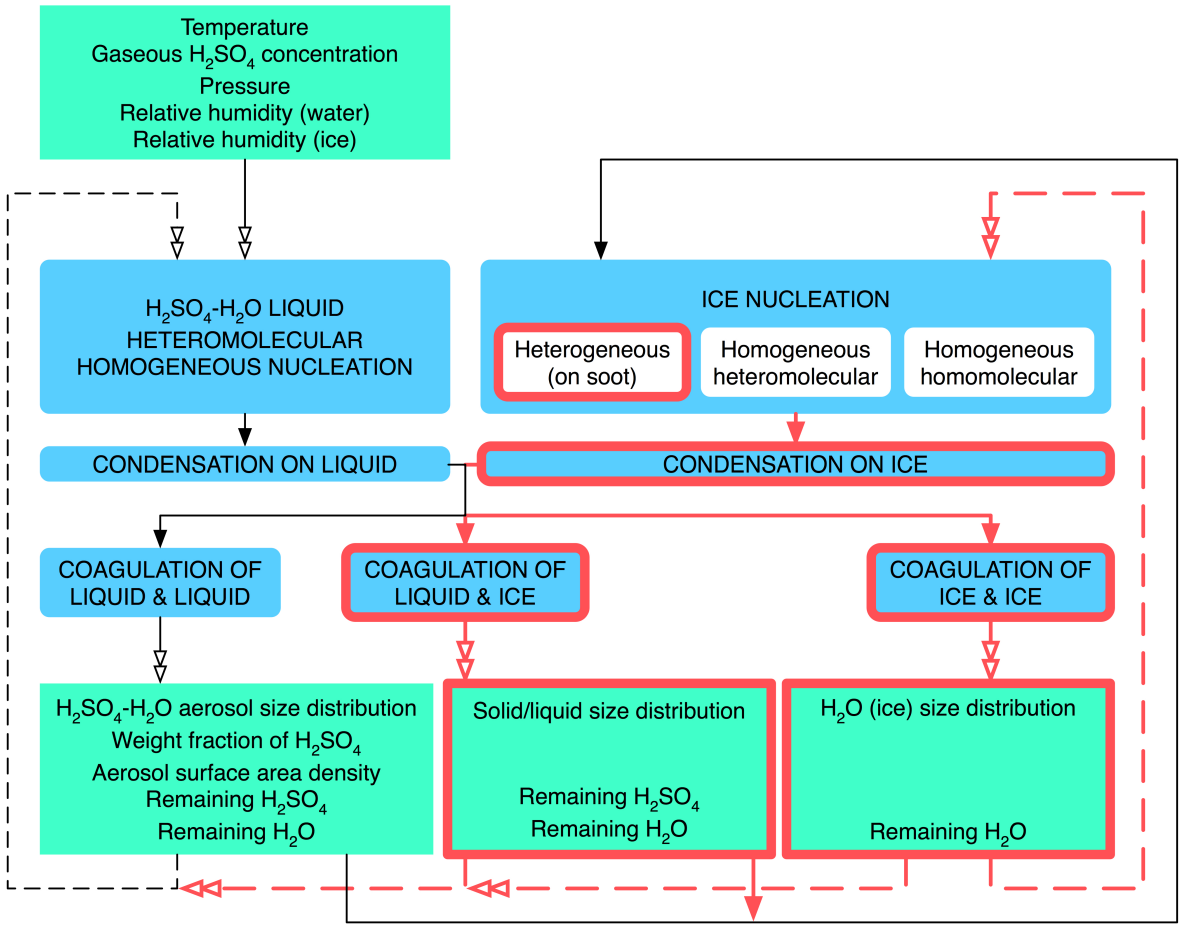

Figure 5.4.1: From Figure 4.5.2. Incomplete sections are outlined in red.

One additional area where SAMM is still lacking is not microphysics, but chemistry. Most fuel sulphur becomes SO_2 upon combustion, with the rest forming fully oxidised sulphur products, S(VI) (SO_3 and H_2SO_4). Further S(VI) is produced by reactions of SO_2 with OH, $H_2O$and oxygen inside the engine. Once emitted into the plume, SO_2 undergoes oxidation and forms SO_3, a step which is limited by the availability of OH. SO_3 then reacts with water relatively quickly (< 1 s) to form H_2SO_4 [Penner et al., 1999]. The non-H_2SO_4 sulphur compounds present in aircraft plumes therefore contribute to ice nucleation by eventually becoming H_2SO_4, consequently sulphur chemistry needs to be included in SAMM in order to accurately reflect this addition. A version of SAMM with sulphur chemistry has already been used to model volcanic eruption [Tahir, 2005, Tahir et al., 2006] and another version of SAMM with sulphur capability is being developed by Tripathi [2005]. Investigation into the suitability of each scheme will occur before one is chosen for inclusion in SAMM.

Chapter 6

Conclusions

The preceding year's aims were to establish a plan by which the eventual goal of producing global maps of aircraft induced cirrus could be accomplished, and to start acting upon the plan. Thus far, the following has been achieved:

- The evolution of emissions into eventual contrail cirrus has been shown as consisting of various processes, chemical, microphysical and dynamical (Table 3.3.2). From this, a set of tasks have been outlined which will accomplish the aim of producing global maps of aircraft induced cirrus (Figure 4.1.1).
- Data sets for flight maps (Figure 4.2.1) and atmospheric data (temperature, pressure, relative humidity) have been acquired and used as model inputs.
- Cirrus climatologies from HIRS and ISCCP have been acquired and plotted (Figures 4.3.1, 4.3.2).
- A contrail formation model has been created which applies the Schmidt-Appleman criterion globally. It predicts contrail formation in those areas where aircraft have passed and atmospheric conditions are suitably cold and moist (Figure 4.4.1).
- A microphysical model (SAMM) capable of simulating the life cycle of H_2SO_4-H_2O aerosol has been modified to allow for homomolecular and heteromolecular homogeneous ice nucleation (Appendix A). A plan has been drawn up for how to modify the model further such that other processes present in plumes may be simulated (Figures 4.5.2).

All three models as well as their input data require updates and additions. The following are planned for completion over the proceeding two years:

- Flight data (TRADEOFF) will be replaced by the more modern and complete AERO2k data set.
- Initialisation data for atmospheric parameters will be complemented with NCEP global data to allow comparison with parallel efforts in this area [Lim, 2005, Lim et al., 2006]. Methods currently in use for extracting ERA40 data will be refined to allow for less interpolation, increasing accuracy.

- Cirrus climatologies from GRAPE and MIPAS will complement those currently acquired.
- An algorithm will be created which calculates simulated contrail cirrus as a fraction of total cirrus. For all climatologies from which total cirrus may be calculated, errors and uncertainties will be required. Quantifying contrail cirrus fraction will only be pertinent if the fraction exceeds the uncertainty in a climatology's total cirrus coverage.
- The contrail model will make use of a parameterisation by Sausen et al. [1998] for predicting percentage cover produced by contrail cirrus from the Schmidt-Appleman criterion. This will help produce maps of contrail cirrus which can be directly compared to cirrus climatologies. The contrail model also needs to produce output which can be used as input directly by SAMM.
- The Stratospheric Aerosol Microphysical Model (SAMM) will require additions of:
  - Sulphur chemistry such that non-H_2SO_4 sulphur compounds from the exhaust can be correctly accounted for.
  - Heterogeneous nucleation of ice from soot, one of the main precursors to ice particles in contrails.
  - Condensation and evaporation of H_2O and H_2SO_4 on to and from ice particles.
  - Coagulation between all types of particles (solid, liquid and mixed solid and liquid).

Of the three models, the contrail model is nearly complete and requires minor changes and additions to make use of new data and refine its output. These changes will continue to be made as data becomes available. Progress is needed on SAMM to render it capable of simulating ice and ice-liquid processes. Since ice is the sole ingredient of cirrus, changes in SAMM will be prioritised from September 2006 and it is hoped that SAMM can be ready by September 2007. Efforts will also be aided by expertise from collaborators abroad [Tripathi, 2005, Vancassel, 2005]. The model which will compare simulated contrail cirrus with real cirrus from climatologies requires significant additions, both in terms of data and comprison method. Progress and completion of this model is largely dependant on output from the other two models, so whilst climatologies will be acquired, algorithms for comparison will only be investigated in 2007 once microphysical model and contrail model output is reliable.

Of the four aims listed at the start of the report, these have been satisfactorily achieved and it is hoped that further work will be accomplished on schedule. The author remains grateful to the UK Department for Transport for funding this project.

Appendix A

Parameterisation details

For algorithms in SAMM, see Tripathi et al. [2004].

A.1 Homogeneous homomolecular ice nucleation by Koop et al. [2000]

The nucleation rate J for ice in cm^{-3} s^{-1} is parameterised thus:

$$\ln J = -906.7 + 8502\Delta - 26924\Delta^2 + 29180\Delta^3, \tag{A.1.1}$$

where Δ is a difference in H_2O activities, parameterised:

$$\Delta = \alpha \exp\left[\frac{\beta}{RT}\right] - \gamma. \tag{A.1.2}$$

α is the activity of water and γ the activity of water in equilibrium with ice. β is just an intermediate variable:

$$\begin{aligned}\beta = \quad & A\left[p - \frac{C}{2}p^2 - \frac{1}{6}\frac{\partial C}{\partial p}p^3\right] \\ & -B\left[p - \frac{D}{2}p^2 - \frac{1}{6}\frac{\partial D}{\partial p}p^3\right],\end{aligned} \tag{A.1.3}$$

$$\gamma = \exp\left(\frac{1}{RT}\left[210368 + 131.438T - 3.32373 \times 10^6 T^{-1} - 41729 \ln T\right]\right). \tag{A.1.4}$$

Molar volumes A and B are:

$$A = -230.76 - 0.1478T + 4099.2T^{-1} + 48.8341 \ln T \tag{A.1.5}$$

$$B = 19.43 - 2.2 \times 10^{-3}T + 1.08 \times 10^{-5}T^2, \tag{A.1.6}$$

with isothermal compressibilities C and D defined:

$$C = 1.6 \ -8.8 \ p \tag{A.1.7}$$

$$D = 0.22 - 0.17p. \tag{A.1.8}$$

We have therefore defined J, the homomolecular homogeneous nucleation rate for ice as a function of atmospheric pressure and temperature.

Equation in which first used	Symbol	Description	Units
A.1.1	J	Rate of ice nucleation	particles s^{-1}
	Δ	Valid for $0.26 < \Delta < 0.34$, $\Delta = a_w - a_w^i$, the difference between the activity of water and the activity of water in equilibrium with ice	[Unitless]
A.1.2	α	The activity of water at temperature T and zero pressure	[Unitless]
	β	Intermediate variable	[n/a]
	γ	The activity of water in equilibrium with ice as a function of T and p	[Unitless]
	R	Gas constant (8.314472)	J K mol^{-1}
	T	Temperature, valid for $170 < T < 240$	K
A.1.3	p	Mechanical pressure in Gigapascals ($0 < p < p_{max}$)	GPa
	p_{max}	Maximum valid pressure, $p_{max} \simeq -0.93 + 1.37 \times 10^{-2} T - 4.12 \times 10^{-5} T^2$	GPa
	A	Molar volume of pure liquid water	cm^3 mol^{-1}
	B	Molar volume of pure ice	cm^3 mol^{-1}
	C	Isothermal compressibility of water	GPa^{-1}
	D	Isothermal compressibility of ice	GPa^{-1}

Table A.1.1: Parameters used in homomolecular homogeneous ice nucleation by Koop et al. [2000].

A.2 Homogeneous heteromolecular ice nucleation by Tabazadeh et al. [1997, 2000]

The rate of nucleation J for ice from droplets of H_2SO_4-H_2O of volume V_d in cm^{-3} s^{-1} is defined [Tabazadeh et al., 1997]:

$$J = J(T, w_s, V_d) = C \exp\left[\frac{-\Delta F_g - \Delta F_{act}}{kT}\right]. \tag{A.2.1}$$

The pre-exponential factor C is estimated:

$$C \simeq 2.1 \times 10^{33} V_d \sqrt{\sigma_{sul/ice} T}, \tag{A.2.2}$$

whilst the Gibbs free energy ΔF_g and the diffusion activation energy ΔF_{act} are:

$$\Delta F_g = \frac{4}{3} \pi \sigma_{sul/ice} r_g^2, \tag{A.2.3}$$

$$\begin{aligned} \Delta F_{act} \times 10^{13} = \; & 1.1992475202 \times 10^4 \\ & -5.2298196745 \times 10^2 \; T \; +8.2328420460 \times 10^0 \; T^2 \\ & -6.4173902638 \times 10^{-2} T^3 + 2.6889968134 \times 10^{-4} \; T^4 \\ & -5.8279763451 \times 10^{-7} T^5 + 5.1479983159 \times 10^{-10} T^6. \end{aligned} \tag{A.2.4}$$

The interface energy $\sigma_{sul/ice}$ is approximated:

$$\sigma_{sul/ice} \simeq |\sigma_{sul/air} - \sigma_{ice/air}|, \tag{A.2.5}$$

and the critical ice germ radius r_g is defined:

$$r_g = \frac{2M_w\sigma_{sul/ice}}{\rho_{ice}\left[L_m \ln\frac{T_f}{T} + \frac{1}{2}R(T+T_f)\ln a_w\right]}. \tag{A.2.6}$$

The remaining unknowns are then an interface energy $\sigma_{sul/air}$, the density of ice ρ_{ice}, latent heat of melting for ice L_m and the activity of water a_w:

$$\sigma_{sul/air} = 142.35 - 0.96525w_s - T(0.22954 - 0.0033948w_s), \tag{A.2.7}$$

$$\rho_{ice} = 0.916 - 8.75\times10^{-5}\Delta T - 1.667\times10^{-7}\Delta T^2, \tag{A.2.8}$$

$$L_m = 10^{-18}(19.04 + 0.05793\Delta T - 1.9907\times10^{-4}\Delta T^2) \tag{A.2.9}$$

$$\begin{aligned} a_w = {} & 1.0119 && -2.1855\times10^{-2}\ \ln PP \\ & -3.2418\times10^{-2}(\ln PP)^2 && -6.6310\times10^{-3}(\ln PP)^3 \\ & -6.4073\times10^{-4}(\ln PP)^4 && -2.3609\times10^{-5}(\ln PP)^5. \end{aligned} \tag{A.2.10}$$

This leaves the H_2SO_4 fraction of a droplet by weight w_s:

$$\begin{aligned} w_s = {} & -1.9088\times10 && -1.8112\times10\ \ln PP \\ & -2.1913\ (\ln PP)^2 && +4.8128\times10^{-2}(\ln PP)^3 \\ & +3.0381\times10^{-2}(\ln PP)^4 && +1.6617\times10^{-3}(\ln PP)^5. \end{aligned} \tag{A.2.11}$$

Equations A.2.1 to A.2.11 constitute a method to calculate the the rate of formation of ice particles from H_2SO_4-H_2O aerosol, requiring inputs of ambient temperature, H_2SO_4-H_2O droplet volume, activity of water for droplet size, pressure and partial pressure of water vapour. The method was updated [Tabazadeh et al., 2000] with the following refinements to L_m, $\sigma_{sul/air}$ and ΔF_{act}:

$$L_m = 10^7[6005.2356 + 18.2719\Delta T - 0.06354\Delta T^2], \tag{A.2.12}$$

$$\begin{aligned} \sigma_{sul/air}(180 \le T \le 220) &= \sigma_{220} + (5.5 - 0.025T)(\sigma_{180} - \sigma_{220}) \\ \sigma_{sul/air}(220 < T \le 260) &= \sigma_{260} + (6.5 - 0.025T)(\sigma_{220} - \sigma_{260}), \end{aligned} \tag{A.2.13}$$

$$\begin{aligned} \Delta F_{act}(T \le 220)\times10^{13} = {} & -17459.516183 \\ & +458.45827551\ T\ -4.8492831317\ T^2 \\ & +0.026003658878\ T^3 - 7.1991577798\times10^{-5}\ T^4 \\ & +8.9049094618\times10^{-8}T^5 - 2.4932257419\times10^{-11}T^6 \end{aligned} \tag{A.2.14}$$

$$\begin{aligned} \Delta F_{act}(T > 220)\times10^{13} = {} & 104525.93058 \\ & -1103.7644651\ T\ +1.070332702\ T^2 \\ & +0.017386254322\ T^3 - 1.5506854268\times10^{-6}\ T^4 \\ & -3.2661912497\times10^{-8}T^5 + 6.467954459\times10^{-10}T^6. \end{aligned} \tag{A.2.15}$$

The remaining variables (interface energies in dyn cm^{-1}) are defined:

$$\begin{aligned}
\sigma_{180} = \; & 85.75507114 \; + \; 9.541966318\times10^{-2}w \\
& - \; 1.103647657\times10^{-1}w^2 + 77.485866933\times10^{-3}w^3 \\
& - \; 1.912224154\times10^{-4}w^4 + \; 1.736789787\times10^{-6}w^5 \\
\sigma_{220} = \; & 82.01197792 \; + \; 5.312072092\times10^{-1}w \\
& - \; 1.050692123\times10^{-1}w^2 + \; 5.415260617\times10^{-3}w^3 \\
& - \; 1.145573827\times10^{-4}w^4 + \; 8.969257061\times10^{-7}w^5 \\
\sigma_{260} = \; & 77.40682664 \; - \; 6.963123274\times10^{-3}w \\
& - \; 9.682499074\times10^{-3}w^2 + \; 8.87979880 \; \times10^{-4}w^3 \\
& - \; 2.384669516\times10^{-5}w^4 + \; 2.095358048\times10^{-7}w^5, \qquad \text{(A.2.16)}
\end{aligned}$$

where w denotes the H_2SO_4 fraction of the droplet by weight.

Currently, both parameterisations have been implemented and the updated one has been checked against code from the author.

Equation in which first used	Symbol	Description	Units
A.2.1	J	Rate of ice nucleation	particles s^{-1}
	C	Pre-exponential factor	particles s^{-1}
	ΔF_g	Gibbs free energy for ice germ formation	erg (g cm^2 s^{-2})
	ΔF_{act}	Diffusion activation energy of H_2O molecules across the ice/sulphate solution phase boundary	erg
	k	Boltzmann constant ($1.3806503 \times 10^{-23}$)	m^2 kg s^{-2} K^{-1}
	T	Ambient temperature	K
A.2.2	V_d	Volume of H_2SO_4-H_2O solution droplet	cm^3
	$\sigma_{sul/ice}$	Interface energy between sulphate solution and ice	dyn(g cm s^{-2}) cm^{-1}
A.2.3	r_g	Critical germ radius	cm
A.2.5	$\sigma_{sul/air}$	Interface energy between sulphate solution and air	dyn cm^{-1}
	$\sigma_{ice/air}$	Interface energy between sulphate ice and air (~ 105)	dyn cm^{-1}
A.2.6	M_w	Molecular weight of water (18.02)	g mol^{-1}
	ρ_{ice}	Density of ice	g cm^{-3}
	L_m	Latent heat of melting ice	erg mol^{-1}
	T_f	Melting temperature of ice (273.15)	K
	R	Universal gas constant (83144720)	erg mol^{-1} K^{-1}
	a_w	Activity of water	[Unitless]
A.2.7	w_s	Weight percent of H_2SO_4-H_2O solution droplet	%
A.2.8	ΔT	$\Delta T = T - T_F$	K
A.2.10	PP	Atmospheric partial pressure of water vapour	mb

Table A.2.1: Parameters used in heteromolecular homogeneous ice nucleation from H_2SO_4-H_2O solutions by Tabazadeh et al. [1997, 2000].

Appendix B

Additional work

A poster produced by Lim et al. [2006] for the international Transport, Atmosphere & Climate conference [*As yet undecided*, 2006] is included on the next page.

Comparison of cirrus cloud coverage calculated from reanalysis meteorological data compared with satellite data

L.L. Lim[1], D.S. Lee[1,2], R. Tahir[2], R.G. Grainger[2], K. Gierens[3] and M. Ponater[3]

[1] Dalton Research Institute, Dept of Environmental & Geographical Sciences, Manchester Metropolitan University, UK
[2] Sub-Department of Atmospheric, Oceanic and Planetary Physics, University of Oxford, UK
[3] Institute for Atmospheric Physics, Deutsches Zentrum für Luft and Raumfahrt (DLR), Oberpfaffenhofen, Germany

Introduction

- The IPCC 'Aviation and the Global Atmosphere' report (1999) identified contrails and cirrus clouds as having potentially the largest effects of aviation on radiative forcing. This work forms part of a wider investigation to identify the sources of uncertainties in estimating radiative forcing from contrails.
- Cirrus coverage is required to determine how much of the potential contrail coverage is actually free for contrails. Therefore, it is important to compare calculated cirrus cloud coverage with observations.

Cirrus cloud parameterisation

- A method to calculate contrail coverage has previously been published by Sausen et al. (1998). The first stage of this work uses the aforementioned methodology to produce an offline model that calculates the cirrus cloud coverage from different sources of meteorological data.

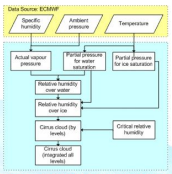

Fig 1: ECHAM cirrus cloud parameterisation

- It is necessary to have access to sufficiently resolved meteorological data in time and space. The ECMWF ERA-40 reanalysis data sets fulfil these criteria. From these data sets, potential fractional cirrus cloud coverage is calculated from specific humidity and temperature data using a parameterisation similar to that adopted for the general circulation model, ECHAM (Chen and Roeckner, 1997).

Satellite data

- The International Satellite Cloud Climatology Project (ISCCP) was established in 1982 to produce global, reduced resolution datasets of basic properties of the atmosphere from which cloud parameters could be derived (Rossow et al., 1996).
- Five geostationary and two polar orbiting satellites have been used to infer the global distribution of cloud properties and their diurnal, seasonal and inter-annual variations.
- The ISCCP analysis correlates radiances measured by satellites with TOVS temperature, humidity, ice and snow to determine information about clouds and the surface.
- Satellites (apart from TOVS) which cover January 1999 are NOAA-12, NOAA-14, GOES-8, METEOSAT-5 and GMS-5.

Data specification

Table 1: Data used in the comparison study

	Meteorology	Satellite
Dataset	ECMWF ERA-40	ISCCP climatological summary product (D2)
Parameters	Specific humidity and temperature	Daytime cloud (cirrus) amount (%)
Year	January 1999	January 1999
Horizontal resolution	2.5 x 2.5 degrees globally	280 km equal area grid, longitudinally 2.5 degrees
Vertical range	500 to 50 hPa	440 to 50 hPa
Temporal resolution	Monthly mean calculated from 00, 06, 12 and 18 UTC	Monthly mean calculated from 00, 03, 06, 09, 12, 15, 18 and 21 UTC

Results and Discussion

- The resulting cirrus cloud coverage (Fig 2) is compared with observed global cloud data from the ISCCP dataset (Fig 3).

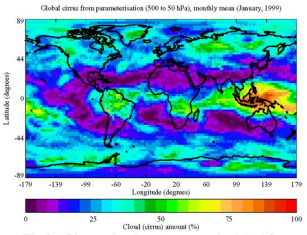

Fig 2: Cirrus cloud coverage calculated from ERA-40 data using ECHAM parameterisation

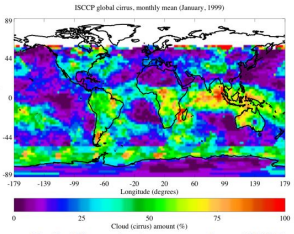

Fig 3: Cirrus cloud coverage from ISCCP

- Calculated and ISCCP cirrus data for latitudes > -45° and latitudes < 45° were used in this comparison study. This is due to unavailable / inappropriate ISCCP data for latitudes outside this range.
- High coverage values were calculated over Polynesia in the Pacific Ocean, Amazon basin, central Africa and along the Inter Tropical Convergence Zone (ITCZ). This is similar to the ISCCP data, even though the ISCCP cirrus coverage in these areas was higher and extends further in extent than that calculated from the ERA-40 data.
- Low coverage values were calculated over the East Pacific Rise, Central America, North Africa and India. Similar structures were observed in the ISCCP data. Again, the ISCCP data have higher values.

Table 2: Comparison of coverage statistics for latitudes between -45° and 45°

Statistic	Parameterisation	ISCCP
Minimum	0 %	0 %
Maximum	92 %	99 %
Mean	24 %	30 %

- Table 2 shows that ISCCP has a higher maximum coverage and mean value than the calculated coverage from ERA-40.
- It is known that the ECMWF model underestimates humidity data in the upper troposphere (Ovarlez et al., 2000).

Conclusions and further work

- This comparison study highlights the sensitivity of meteorological data used in calculating global cirrus coverage. Cirrus cloud coverage is an important parameter in estimating the uncertainties for contrail coverage, as it is required to determine how much of the potential contrail coverage is actually free for contrails.
- Planned further work includes comparison of calculated coverage from other meteorological dataset with satellite data; comparisons of different temporal statistics (diurnal, seasonal and inter-annual variations) and detailed comparisons over specific regions.

References

Chen CT and Roeckner E (1997) **Cloud simulations with the Max-Planck-Institute for Meteorologie general circulation model ECHAM4 and comparison with observations**. J. Geophys. Res., 102 9335-9350

IPCC (1999) **Aviation and the Global Atmosphere**, Penner JE, Lister DH, Griggs DJ, Dokken DJ and McFarland M (eds). Intergovernmental Panel on Climate Change, Cambridge University Press, UK.

Ovarlez J, van Velthoven P, Sachse G, Vay S, Schlager H and Ovarlez H (2000) **Comparison of water vapor measurements from POLINAT2 with ECMWF analyses in high-humidity conditions.** J. Geophys. Res. 105, 3737-3744.

Rossow WR, Walker AW, Beuschel DE and Roiter MD (1996) **International Satellite Cloud Climatology Project (ISCCP) documentation of new cloud datasets**. Science Systems and Applications Inc. at NASA Goddard Institute for Space Studies.

Sausen R, Gierens K, Ponater M and Schumann U (1998) **A Diagnostic Study of the Global Distribution of Contrails Part 1: Present Day Climate**. Theor. Appl. Climatol. 61, 127-141

Centre for Air Transport and the Environment, Department of Environmental and Geographical Sciences, Manchester Metropolitan University, Manchester, M1 5GD, UK, Tel: +44 161 247 3653, Fax: +44 161 247 6332, E-mail: l.lim@mmu.ac.uk, WWW: www.mmu.ac.uk/cate

Appendix C

Aerodynamic contrails

Aerodynamic contrails do not originate from the thermodynamics encapsulated in the Schmidt-Appleman criterion (covered in §3.3). They can form even above 0°C. Thermodynamic condensation trails normally correspond in number to the engines mounted on a craft: this is not true of aerodynamic contrails for which the cause is the body of the aeroplane itself (see Figure C.0.1).

Figure C.0.1: An example of aerodynamic contrails [Gierens, 2006a].

Aerodynamic contrails are typically observed at low altitudes in humid air. Schumann [1996] explains how vertices which trail wingtips (or propellors) can cause adiabatic cooling of roughly 15 K at uper tropospheric conditions [Gierens, 2006a]. This translates to a ΔRH several hundred percent, leading to contrails. The effect requires frost saturation or supercooled droplets and is stronger for shorter wingspan, faster aircraft and engines closer to the vortex axis. Aerodynamic contrails are therefore of limited concern for subsonic aircraft, but may be of considerable interest for supersonic designs.

Since they are observed only rarely and therefore of little practical importance [Schumann, 2005], aerodynamc contrails are not considered in this present work.

References

H Appleman. The formation of exhaust condensation trails by jet aircraft. *Bulletin of the AMS*, 34(1):14–20, 1953.

A Brewer. The stratospheric circulation: a personal history. `http://www.aero.jussieu.fr/~sparc/News15/15_Norton.html`, 1999.

M Constable. Canadian air aces and heroes. `http://www.constable.ca/turner.html`, 2006.

C J Eyers, P Norman, J Middel, M Plohr, S Michot, K Atkinson, and R A Christou. *AERO2k global aviation emissions inventories for 2002 and 2025*, 2004.

K Gierens. Contrails, contrail-cirrus, and ship tracks. In *As yet undecided* [2006]. *Unpublished, provisionally* Transport, Atmosphere and Climate Proceedings.

K Gierens. Personal communication, 2006b.

A Heymsfield. Cirrus uncinus generating cells and the evolution of cirriform clouds. Part II: the structure and circulation of the cirrus generating head. *Journal of the Atmospheric Sciences*, 4:809–819, 1975.

A J Heymsfield and G M McFarquhar. Mid-latitude and tropical cirrus: microphysicl properties. In Lynch et al. [2002], pages 78–101. ISBN 0 19 513072 3.

M Z Jacobson. Numerical techniques to solve condensational and dissolutional growth equations when growth is coupled to reversible reactions. *Aerosol Science and Technology*, 27:491–498, 1997.

M Z Jacobson, editor. *Fundamentals of atmospheric modelling*. Cambridge University Press, 1999. ISBN 0 521 63717 1.

M Z Jacobson. Analysis of aerosol interactions with numerical techniques for solving coagulation, nucleation, condensation, dissolution, and reversible chemistry among multiple size distributions. *Journal of Geophysical Research*, 107(D19):4366, 2002.

M Z Jacobson, R P Turco, E J Jensen, and O B Toon. Modeling coagulation among particles of different composition and size. *Atmospheric Environment*, 28(7):1327–2310, 1994.

B Karcher. A trajectory box model for aircraft exhaust plumes. *Journal of Geophysical Research*, 100(D9):18,835–18,844, 1995.

B Karcher. Aviation-produced aerosols and contrails. *Surveys in Geophysics*, 20:113–167, 1999.

B Karcher and U Lohmann. A parameterization of cirrus cloud formation: heterogeneous freezing. *Journal of Geophysical Research*, 108(D14):4402, 2003.

T Koop, B Luo, A Tsias, and T Peter. Water activity as the determinant for homogeneous ice nucleation in aqueous solutions. *Nature*, 406, 2000.

D S Lee. Personal communication, 2005.

L L Lim. Personal communication, 2005.

L L Lim, D S Lee, R Tahir, R G Grainger, K Gierens, and M Ponater. Comparison of cirrus cloud coverage calculated from reanalysis meteorological data compared with satellite data. In *As yet undecided* [2006]. *Unpublished, provisionally* Transport, Atmosphere and Climate Proceedings.

X Liu and J E Penner. Ice nucleation parameterization for global models. *Meteorologische Zeitschrift*, 14(4):499–514, 2005.

D K Lynch. Cirrus: history and definition. In Lynch et al. [2002], pages 3–10. ISBN 0 19 513072 3.

D K Lynch, K Sassen, D O Starr, and G Stephens, editors. Oxford University Press, 2002. ISBN 0 19 513072 3.

As yet undecided, editor. 2006. *Undecided. Unpublished, provisionally* Transport, Atmosphere and Climate Proceedings.

UK Met Office. Learning centre, Secondary Teachers, Clouds. `http://www.metoffice.gov.uk/education/secondary/teachers/clouds.html`, 2006.

P Minnis. Contrails and cirrus clouds. 2005.

P Minnis, J K Ayers, R Palikonda, and D Phan. Contrail, cirrus trends and climate. *American Meteorological Society*, 2003.

NASA. SciJinks, Images for the classroom, Clouds. `http://scijinks.jpl.nasa.gov/en/educators/gallery/clouds_atmos/cirrus_L.jpg`, 2006.

R Paugam, D Cariolle, and R Paoli. Numerical simulations of aircraft plumes using a meso scale code. In *As yet undecided* [2006]. *Unpublished, provisionally* Transport, Atmosphere and Climate Proceedings.

J E Penner, D H Lister, D J Griggs, D J Dokken, and M McFarland, editors. *Aviation and the global atmosphere*. Cambridge University Press, 1999. ISBN 0 521 66404 7.

J Reynolds. Contrail photo gallery. `http://www.goodsky.homestead.com/files/gallery.html`, 2006.

W R Rossow, A W Walker, D E Beuschel, and M D Roiter. *International Satellite Cloud Climatology Project (ISCCP) documentation of new cloud datasets*, 1996.

K Sassen. Cirrus: a modern perspective. In Lynch et al. [2002], pages 11–40. ISBN 0 19 513072 3.

R Sausen, K Gierens, M Ponater, and U Schumann. A diagnostic study of the global distribution of contrails Part I: present day climate. *Theoretical and applied climatology*, 61:127–141, 1998.

E Schmidt. Die entstehung von eisnebel aus den auspuffgasen von flugmotoren. *Schriften der Deutschen Akademie der Luftfahrtforschung*, 44:1–15, 1941.

U Schumann. On conditions for contrail formation from aircraft exhausts. *Meteorologische Zeitschrift*, pages 395–414, 1996.

U Schumann. Contrail cirrus. In Lynch et al. [2002], pages 231–255. ISBN 0 19 513072 3.

U Schumann. Formation, properties and climatic effects of contrails. *Comptes Rendus Physique*, 6:549–565, 2005.

D O'C Starr and M Quante. Dynamical processes in cirrus clouds. In Lynch et al. [2002], pages 375–396. ISBN 0 19 513072 3.

A Tabazadeh, E J Jensen, and O B Toon. A model description for cirrus cloud nucleation from homogeneous freezing of sulfate aerosols. *Journal of Geophysical Research*, 102 (20):23845–23850, 1997.

A Tabazadeh, S T Martin, and J-S Lin. The effect of particle size and nitric acid uptake on the homogeneous freezing of aqueous sulfuric acid particles. *Geophysical Research Letters*, 27(8):1111–1114, 2000.

M R Tahir. Modelling studies and observations of the Mount Hekla eruption of 2000. Master's thesis, University of Oxford, 2005.

M R Tahir, X P C Vancassel, R G Grainger, D E Huton, S E Dean, S N Tripathi, and H L Rogers. Modelling and new satellite observations of the Mount Hekla eruption of 2000. *Under submission*, 2006.

Unknown. `http://www.raggedcastle.com/webcrumbs/archives/cat_photography.html`, 2006.

S N Tripathi. Personal communication, 2005.

S N Tripathi, X P Vancassel, R G Grainger, and H L Rogers. *A fast stratospheric aerosol microphysical model (SAMM): H_2SO_4-H_2O aerosol development and validation*, 2004.

X P C Vancassel. Personal communication, 2005.

H Vehkamaki, M Kulmala, I Napari, K E J Lehtinen, C Timmreck, M Noppel, and A Laaksonen. An improved parameterization for sulfuric acid-water nucleation rates for tropospheric and stratospheric conditions. *Journal of Geophysical Research*, 107 (D22):4622, 2002.

F J Zeleznik. Thermodynamic properties of the aqueous sulfuric acid system to 350 K. *Journal of physical and chemical reference data*, 20(6):1157–1200, 1991.